1-1-2016

Dendrimer-Coated Iron Oxide Theranostic Nanoparticles For Cancer Imaging And Therapy

Duy Khanh Luong
Wayne State University,

DENDRIMER-COATED IRON OXIDE THERANOSTIC NANOPARTICLES FOR CANCER IMAGING AND THERAPY

by

DUY LUONG

THESIS

Submitted to the Graduate School

of Wayne State University,

Detroit, Michigan

in partial fulfillment of the requirements

for the degree of

MASTER OF SCIENCE

2016

MAJOR: PHARMACEUTICAL

SCIENCE

Approved By:

_____

Advisor Date

ACKNOWLEDGMENTS

I would like to express my deep gratitude to my advisor Dr. Arun Iyer for his continuous support, motivation, and patience during my Master's program. I am grateful for the mentorship I received from Dr. Iyer. Without his guidance and persistent help, I would not have completed my thesis research project. Besides my advisor, I would like to extend my appreciation to the rest of my thesis committee: Dr. Fei Chen and Dr. Zhifeng Kou, for their support, encouragement, and their insightful comments.

My sincere thanks also go to Dr. Zhihui Qin, Dr. Michael Joseph Rybak, and Dr. Joshua Reineke for all the help and the research techniques I learned during my laboratory rotations. Those techniques were very beneficial and helped me a lot throughout my scientific research during the Master's program.

Many thanks to all group members from the U-BiND Systems Laboratory. Thanks to Dr. Prashant Kesharwani and Dr. Rahul Deshmukh for helping me with the chemical ordering, for all the research techniques I learned, and for the continuous support. Thanks Dr. Sushil Kashaw, Shaimaa Yousef, Hashem Alsaab, Rami Alzhrani, Ketki Bhise, Kaustubh Gawde, and Zhaoxian Wang, for the great collaboration, for all the fun, and the ups and downs in research that we shared.

I would like to thank Dr. Subhash Padhye and Dr. Fazlul Sarkar for the anticancer compound CDF, Dr. Timothy Stemmler for the usage of the centrifuge, Dr. Zhi Mei for TEM imaging, Dr. Guangzhao Mao and her group for the assistance with AFM analysis, Dr. Olivia Merkel and Steven Jones for the assistance with

FACS, Dr. Anna Moszczynska and her group for the usage of the Digital Imaging system and the assistance with the confocal microscopy, and Dr. Asfar Azmi for the usage of the fluorescent microscopy. My many thanks also go to all the faculty and staff of the Department of Pharmaceutical Sciences, and all my fellow graduate students for providing me support during the two years of my graduate study.

Last but not least, I would like to thank my family and friends for the tremendous support. Without your help, I would not have completed this achievement and I wish to share this success with you.

Table of Contents

List of Figures

targeted SPIONs@FA-PAMAM nanoparticles (with the color change from red to purple indicating the gradual decrease of MR signal intensity). The percentage of signal intensity compared to cells in PBS was plotted as a function of iron concentration indicating the faster internalization with higher decrease in MR signal intensity of the targeted SPIONs@FA-PAMAM.

Figure 7. (a) *In vitro* cytotoxicity assay showing percentage of cell viability observed at 72 h after treating SKOV3 and HeLa cells with various formulations are shown (n=8); (b) MTT assay observed at 72 h after folate receptor blocking and treating of SKOV3 and HeLa cells with SPIONs@PAMAM-CDF and SPIONs@FA-PAMAM-CDF are shown (n=8); (c) Induction of apoptosis in HeLa cells when treated with CDF, SPIONs@PAMAM-CDF, and SPIONs@FA-PAMAM-CDF as evaluated by Annexin V/7-AAD dual staining. An increased percentage of apoptotic cell population was noted when cells were treated with targeted formulation (SPIONs@FA-PAMAM-CDF) as compared to the non-targeted formulation (SPIONs@PAMAM-CDF), suggesting better killing activity of the targeted formulation SPIONs@FA-PAMAM-CDF.

Figure 8. Western blot analysis showing PTEN and NF-κB expression in HeLa cells in control without treatment (CTL), and cells treated with CDF, targeted formulation SPIONs@FA-PAMAM-CDF (T) and non-targeted formulation SPIONs@PAMAM-CDF (NT), (GAPDH expression was used as the protein loading control).

CHAPTER 1 INTRODUCTION

1.1. Background

Cancer is accountable for millions of deaths annually worldwide. According to the American Cancer Society, cancer is the second most common cause of death in the United States. Approximately 1.7 million new cancer cases are expected and about 600,000 Americans are expected to die of cancer in 2016 [1]. Chemotherapy, radiotherapy, and photothermal therapy are the most common treatments for cancer. Chemotherapy is the most common strategy in cancer treatment because of its higher efficacy as compared to other types of treatments [2–5]. In most cases, cancer diagnosis in the early stage is difficult. Most of the patients are diagnosed at the late stage of cancer with a poor prognosis. In the advanced stage of cancer, chemotherapy and radiotherapy are the only options. However, the development of chemotherapeutic drug resistance is the most common reason leading to the failure of cancer treatment. The conventional treatment with the systemic distribution of chemotherapeutics is problematic and shows a significant flow that can make the difference between success and failure [6]. High doses are often required to accumulate adequate amounts of chemotherapeutic agents at the tumor site to achieve desirable therapeutic efficacy. However, larger doses possess a higher risk of adverse side-effects with the increase of toxicity in non-targeted sites or normal tissues. The bleak prognosis for patients diagnosed with metastatic cancer along with the low therapeutic efficacy and the recurrence of cancer in conventional chemotherapy are prompting clinical medicine to adopt a new strategy to detect cancer in early stage and to

deliver the anticancer drugs specifically to tumor site to enhance therapeutic efficiency and minimize side effects.

1.2. CDF (3,4-difluorobenzylidene diferuloylmethane) – a highly potent but extremely lipophilic anticancer drug

In our earlier studies 3,4-difluorobenzylidene diferuloylmethane (CDF), a synthetic analog of a potent flavonoid anticancer compound has shown 16-fold increased half-life and high anticancer activity compared to its natural analog, diferuloylmethane when tested on pancreatic cancer cells [7–9]. The observed improvement in properties of CDF was attributed to its much higher stability and bioavailability compared to the natural counterpart. CDF could inhibit the growth of cancer cells through down-regulation of multiple miRNAs, up-regulation of phosphatase and tensin homolog (PTEN), and attenuation of histone methyltransferase EZH2 [10–12]. These findings strongly indicate that CDF could be a good candidate for several cancers, including cervical cancer. However, one significant problem limiting CDF from further preclinical and clinical testing is its very poor aqueous solubility. In our previous studies, we successfully overcame CDF's solubility problem by using dendrimer and micellar nanocarriers [7,13]. In those studies, CDF has shown a significant anticancer activity on tested cancer cells including triple marker positive stem-like pancreatic cancer cells.

1.3. Polyamidoamine (PAMAM) dendrimers in targeted drug delivery

1.3.1. What are PAMAM dendrimers?

PAMAM dendrimers are a relatively novel class of polymers with a well-defined, nano-sized, highly branched and monodispersed structures with numerous hydrophilic reactive amine groups on the periphery and lipophilic internal cavities. PAMAM dendrimers are known for their ability to encapsulate hydrophobic drugs in their internal cavities to enhance the aqueous solubility of these hydrophobic compounds [14–16]. The larger numbers of reactive amine groups on the periphery makes PAMAM dendrimers suitable for many biomedical applications such as drug conjugation, siRNA and gene complexation, and conjugation to bio-recognition molecules to achieve active targeting ability [17,18]. When PAMAM dendrimers are used as drug carriers, they can enhance the drug biodistribution in tumor site possibly by taking the advantage of enhanced permeation and retention effect [19–21]. In addition, it is demonstrated that by carrying targeting ligands on the surface, PAMAM dendrimers can achieve active receptor targeting. In this regards, one of the most commonly used targeting ligands is folic acid (FA). Many types of cancer cells (such as ovarian, colon, lung, breast and cervical cancer cells) are known to have a high expression of folate receptors on their membranes [22–25]. Drug carriers decorated with FA can achieve targeting ability and high accumulation in cancer cells by taking advantage of the specific binding of FA with folate receptors overexpressed on these targeted cancer cells. Cellular internalization is facilitated via folate-receptor mediated

endocytosis and followed by the release of anticancer drug; thus, resulting in a better accumulation with minimized toxicity to normal cells.

1.3.2. Dendrimer mediated tumor targeted delivery: Passive and active targeting

1.3.2.1. Dendrimer-mediated passive targeting strategy

The passive targeting pathway of dendrimers utilizes the inherent ability of macromolecules to extravasate and accumulate specifically in the tumor microenvironment based on a phenomenon called the enhanced permeability and retention (EPR) effect, which was discovered by Matsumura and Maeda [19]. The EPR phenomenon suggested that the rapid proliferation of tumor cells create complex networks of blood vessels that are highly disorganized and leaky. The dilation of blood vessels is facilitated by excessive levels of vascular permeability mediators secreted by tumor cells [4,26–28]. The anatomical and pathophysiological abnormalities in tumor environment result in an extensive leakage of macromolecules and nanoparticles including dendrimers into the tumor interstitium [26,28–30]. In addition, the lymphatic clearance in solid tumors is dysfunctional in general. As a consequence, drugs conjugated or encapsulated in macromolecules and nanoparticles can attain very high local concentrations in the tumor environment with negligible accumulation in the non-targeted or healthy organs. Particle size is an important factor dictating the localization and retention in tumor tissues. It is observed that nanoparticles in the range of ten to a few hundred nanometers can exploit the EPR phenomenon to accumulate in tumor tissues [31]. In this regards, dendrimers with a typical size range from 10 to 20 nm

are favorable to achieve passive tumor targeting [32]. In addition, dendrimers have prolonged half-life in the systemic circulation and can avoid renal excretion due to the ability to bind to plasma proteins and biomolecules [33]. As a result, dendrimers can retain in the blood for an extended duration and accumulate in the tumor environment by EPR effect, suggesting a sustained and controlled delivery profile.

1.3.2.2. Dendrimer-mediated active targeting strategy

The passive tumor targeting has numerous challenges due to the complexity of the anatomic and pathophysiological barriers in the *in vivo* biological environment. The passive targeting strategy is only effective in highly permeable solid tumors. In most cases, the permeability in tumors is relatively poor and non-uniform; thus, it is difficult to take advantage of EPR effect in these heterogeneous and impermeable tumors [34]. These limitations can be resolved to some extent by utilizing the active targeting strategy, a phenomenon where specific targeting ligands are introduced to the nanostructure to facilitate the selective binding to unique and overexpressed receptors on specific tumor cells. In this regards, dendrimers with numerous reactive functional groups on the periphery are favorable for the conjugation with targeting ligands for the active targeting effect.

Folic acid is one of the most common targeting ligands for several reasons. Folic acid is a low molecular weight B-vitamin whose receptors are found to be overexpressed in numerous types of cancer cells, including lung, breast, colon, choroid plexus brain, choriocarcinoma, cervical, and ovarian cancers [22,24,35]. Folate receptors are known to occur in clusters, giving the ability to enhance targeting efficacy by using multiple folic acid moieties on nanoparticles. Many types

of cancer cells are known to have a high level expression of folate receptors. Healthy cells also express folate receptors but with a significantly lower degree. Moreover, folate receptors in healthy cells are in a different location which is not accessible from the bloodstream, suggesting that folate receptors in cancer cells could be a perfect target for actively targeted drug delivery [22].

Because of the small size, folic acid is known to be a stable molecule that does not induce an immune response. As compared to an antibody, folic acid is a better targeting ligand since its binding affinity to folate receptors is not diminished after its conjugation to macromolecules or nanoparticles [36,37]. In addition, antigen expression may change over time; whereas, folate receptors are stable because folic acid is a crucial ingredient in biosynthesis needed for cellular proliferation [37–39]. After the binding of the folate-decorated nanoparticles, endocytosis will occur resulting in the internalization of the folate-decorated nanoparticles. Then, folate receptors are recycled to the cell surface and ready for binding with the next nanoparticles [40].

1.4. Biomedical application of Magnetic Resonance Imaging

1.4.1. Magnetic resonance imaging (MRI)

MRI is one of the most common clinical diagnostic tools due to its noninvasive, tomographic properties that offers superb spatial resolution without the dangers of ionizing radiation. Hydrogen nuclei or protons in water molecules are the main contributors to MRI signal in biological applications. In a simplistic sense, MR imaging is just the proton nuclear magnetic resonance (NMR) in the biological systems which yields the intensity maps of the proton relaxation time in

tissue [41]. The difference in the proton density and the relaxation time constants in the tissue samples gives the contrast in the resulting MR images. However, the sensitivity of the MR images is relatively low if we only rely upon these inherent contrast mechanisms [42]. This limitation can be addressed by using exogenous magnetic agents or contrast agents which can influence the spin relaxation time of the local protons thereby enhancing the contrast in the resulting MR images [43–46].

1.4.2. MRI contrast agents

Among several types of contrast agents, the two major classes are chelated paramagnetic ions such as Gadolinium (Gd), and superparamagnetic iron oxide nanoparticles (SPIONs). SPIONs have several advantages as compared to chelated paramagnetic ions. SPIONs are detectable at nM concentrations or lower, whereas chelated paramagnetic ions detection concentration is at the mM in order to generate adequate contrast [47]. In addition, paramagnetic chelates need the exchange of water protons in order to produce local contrast effects; whereas, SPIONs can impact a larger region of tissue without the direct contact with water protons by producing magnetic field gradients [39,45,48].

In recent years, magnetic nanoparticles are getting more attention due to their applications in biology and medicine such as enzyme and protein immobilization, magnetic resonance imaging, tissue engineering, magnetic cell tracking and separation, hyperthermia, and targeted drug and gene delivery [49,50]. Drug delivery systems based on magnetic nanoparticle carriers possess the ability of magnetic resonance imaging contrast agents as well as the advanced

properties of nanocarriers such as the enhanced aqueous solubility, increased systemic circulation time, targeting delivery of chemotherapeutic drugs with reduced toxicity in normal tissues. Magnetic iron oxide (Fe_3O_4) nanoparticles, especially superparamagnetic iron oxide nanoparticles, have been widely studied and shown great potentials in biotechnology because of their biocompatible, inert, and excellent superparamagnetism properties [51,52]. In *in vivo* applications, the surface of these magnetic nanoparticles can be modified with polymeric shells such as dextran, PEG, chitosan, and dendrimers [53–55]. These polymeric shells provide not only the biocompatibility for the magnetic nanoparticles, but also the ability for conjugation with biomolecules such as proteins, nucleic acids, enzymes, targeting ligands, and drugs [56–59].

1.4.3. Iron oxide nanoparticles – Safe and highly effective MRI contrast agents

There are many factors that make iron oxide Fe_3O_4 excellent MRI contrast agents. Iron oxide particles occur naturally in many animals and are currently the only inorganic contrast particles approved for *in vivo* human applications (Endorem® or Feridex I.V.®; Advanced Magnetics, Cambridge, Massachusetts, USA) [39,60,61]. Iron oxide particles are biodegradable without either acute or chronic toxicity [62–65]. Uncoated magnetic iron oxide particles have an LD_{50} of 300 to 600 mg iron per kg body weight, and the surface coating has shown to be able to improve the biocompatibility of the iron oxides by an order of magnitude [39,66]. The typical clinical dose for SPIONs is 1 mg Fe per kg body weight which is significantly lower than LD_{50}. It is also a small fraction of the approximately 3500

mg of total iron in various forms naturally found in the human body. In addition, many studies have shown that the human body has established methods to metabolize the excess amount of iron introduced by the particles [48,64,67,68].

SPIONs have been studied with many different agents for actively targeted MRI. In a study by Cheon et al., SPIONs were modified with dimercaptosuccinic acid, followed by the conjugation of Herceptin molecules via the free thiol functional groups on the particles. The targeting ability of the particles was demonstrated *in vitro* with different cell lines with a different level of her2/neu expression. The results showed a decrease in MRI signal intensity with the increase of the expression of her2/neu. In *in vivo* studies using mice bearing a NIH3T6.7 xenograft, SPIONs conjugated Herceptin showed an enhanced contrast in MR signal as compared to SPIONs conjugated with the irrelevant antibodies [69]. Besides antibody, transferrin has been used as a targeting ligand for SPIONs [38,70]. Many studies have suggested that SPIONs decorated transferrin could benefit from the transferrin receptor-mediated endocytosis, resulting in a higher degree of cellular internalization.

Shi's group used folic acid as a targeting moiety for SPIONs for targeted MRI of tumors. SPIONs were synthesized by co-precipitation method. A layer-by-layer self-assembly method was used to functionalize SPIONs with dendrimer decorated folic acid. The results showed an enhanced in cellular uptake of the SPIONs containing folic acid in tumor cells overexpressed folate receptors. MR images showed a higher increase in the contrast when incubating the folate-decorated SPIONs with human epithelial carcinoma cell line (KB cells) indicating

the targeting effect of the conjugates [71]. In a recent study done by Akal et al., SPIONs were functionalized with APTES ((3-Aminopropyl) triethoxysilane), polyethylene glycol (PEG) and folic acid for the targeted delivery of Quercetin for brain cancer. Prussian blue staining and fluorescence spectroscopy studies showed a higher cellular uptake of the SPIONs containing folic acid. The Quercetin loaded folate-decorated SPIONs showed a higher anticancer activity when tested on U87 cell line (brain adenocarcinoma cells, which have high expression of folate receptors), as compared to L929 cell line (fibroblast cells, which are folic acid receptors negative cells). The results are in accordance with previous studies, suggesting SPIONs modified with appropriate targeting ligands could result in a better accumulation in tumor cells which possess complementary receptor binding domains.

1.5. SPIONs coated FA-PAMAM as a multifunctional agent for cancer imaging and therapy

In this study, SPIONs were synthesized by coprecipitation method, followed by surface coating and fabrication of PAMAM-decorated FA. The magnetic nanocarriers were used to encapsulate a poorly aqueous soluble but highly potent anticancer drug 3,4-difluorobenzylidene diferuloylmethane (CDF), a synthetic analog of a potent flavonoid anticancer compound diferuloylmethane. In our previous studies, CDF has shown a high anticancer activity when tested on pancreatic, cervical, ovarian and lung cancer cells [7–9,72]. The improvement in anticancer properties of CDF was attributed to a 16-fold increased half-life, a higher stability, and bioavailability as compared to its natural counterpart. CDF has

shown to be able to inhibit the growth of cancer cells through down-regulation of multiple miRNAs, up-regulation of phosphatase and tensin homolog (PTEN), and attenuation of histone methyltransferase EZH2 [10–12]. The theranostic capability for cancer imaging and therapy of the magnetic nanocarriers encapsulated CDF was examined by *in vitro* biological studies, cellular uptake, and T_2 relaxation studies. The results demonstrated that the synthesized magnetic nanocarriers could be promising carriers in active targeting cancer imaging and therapy (Fig. 1).

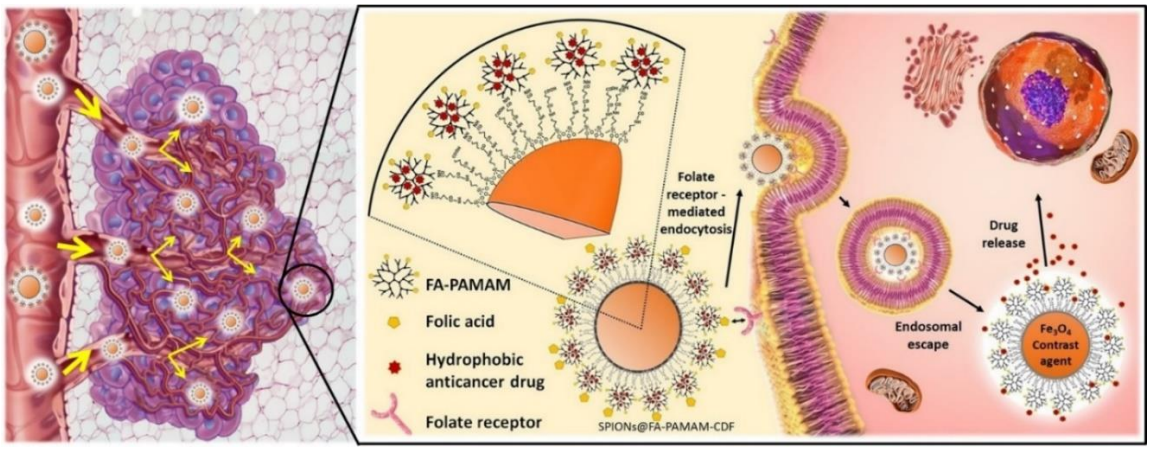

Figure 1. The pictorial representation of accumulation of targeted formulation (SPIONs@FA-PAMAM-CDF) at the tumor site by EPR-effect, followed by folate receptor mediated endocytosis of the formulation due to the specific binding of FA to folate receptors overexpressed on cancer cells.

CHAPTER 2 EXPERIMENTAL DESIGN

2.1. Materials

2.1.1. Reagents

CDF was synthesized as described earlier [7,13]. Fourth generation (4.0G) PAMAM dendrimer, ferrous chloride ($FeCl_2.4H_2O$), ferric chloride ($FeCl_3.6H_2O$), N-(3-(dimethylamino) propyl)-N-ethylcarbodiimide hydrochloride (EDC), and 3-[4,5 dimethylthiazol-2-yl]-2,5diphenyltetrazolium bromide (MTT) was purchased from Sigma-Aldrich (St. Louis, MO). FA was purchased from Fisher Scientific. Guava Nexin Reagent for cell apoptosis kit was purchased from EMD Millipore. All other chemicals were of reagent grade and used without any modification.

2.1.2. Cell lines

Human cervical cancer cells (HeLa cells) and human ovarian carcinoma cells (SKOV3 cells) were used in this study due to their high expression of folate receptors [73–76]. HeLa cells were cultured in Dulbecco's Modified Eagle's Medium (DMEM; Fisher Scientific, Waltham MA) with 10% fetal bovine serum (FBS) and streptomycin sulfate (10mg/L). SKOV3 cells were cultured in Roswell Park Memorial Institute (RPMI) 1640 Medium (Thermo Fisher Scientific, USA) with 10% FBS and streptomycin sulfate (10mg/L). All cell lines were incubated at 37^{o}C in a 5% CO_2 air humidified atmosphere.

2.2. Superparamagnetic iron oxide nanoparticles (SPIONs) synthesis

Superparamagnetic iron oxide nanoparticles (SPIONs) were synthesized using co-precipitation method [77]. Prior to the synthesis, 0.5 M NaOH solution in deionized water (DIW) was prepared in a three-neck 500 ml round bottom flask (RBF) and degassed by bubbling N_2 while stirring at room temperature RT) for 30 min, followed by degas under vacuum while stirring at RT for another 30 min, then was heated to 40^{o}C. Then, ferric chloride $FeCl_3.H_2O$ (6.56 g, 0.024 mol) and ferrous chloride $FeCl_2.4H_2O$ (2.48 g, 0.012 mol) were dissolved in 25 ml of degassed 0.4 M HCl solution in DIW and then added to the RBF through a septum. The RBF was heated at 80^{o}C under strong stirring for 1 h. SPIONs were precipitated using a strong neodymium N52 magnet and then decant the reaction mixture. The SPIONs were washed 5 times by dispersing them back in EtOH (300 ml) with probe sonication for 10 min, followed by magnet precipitation and decant the liquid. A dry powder of SPIONs was obtained by drying under vacuum on a rotary evaporator. The product was characterized by Fourier Transform Infrared Spectroscopy (FTIR). Hydrodynamic size and zeta potential were characterized by dynamic light scattering using Beckman Coulter Delsa Nano.

2.3. FA-PAMAM decorated SPIONs fabrication

FA was conjugated to 4th generation PAMAM dendrimers through carbodiimide coupling chemistry according to our previously reported method [72]. Prior to the FA-PAMAM conjugation, the surface of SPIONs was modified to create

the activated carboxyl groups (Fig 2). The fabrication process includes three main steps: amine functionalization, carboxylation, and FA-PAMAM conjugation.

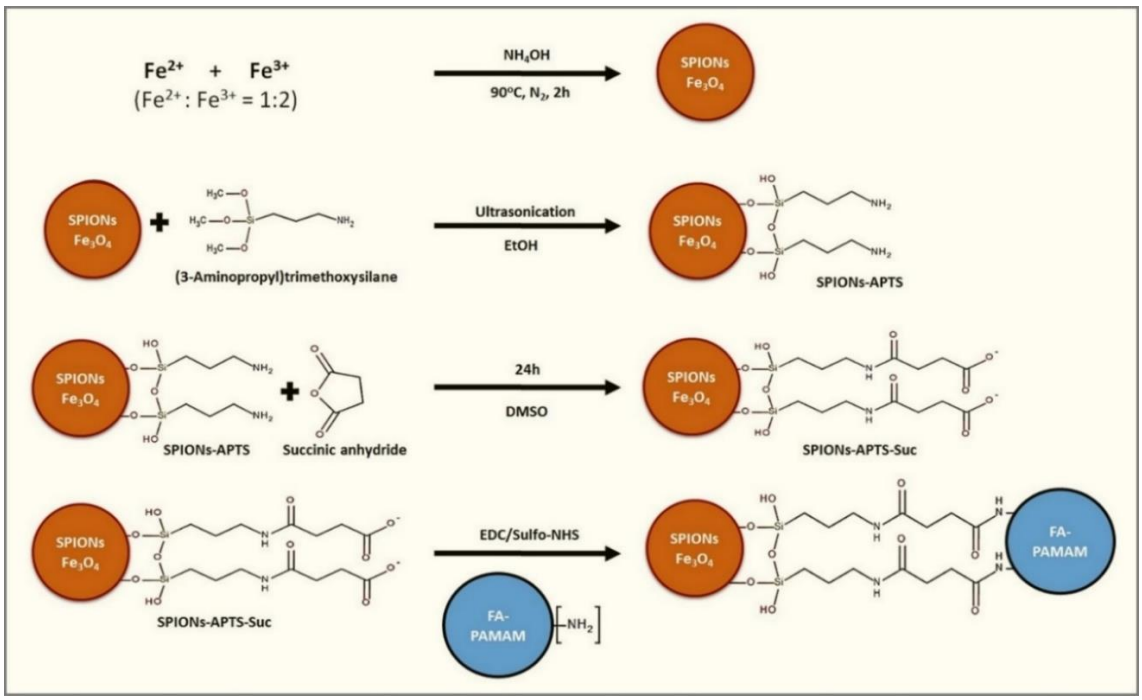

Figure 2. SPIONs decorated FA-PAMAM (SPIONs@FA-PAMAM) fabrication process.

2.3.1. Amine functionalized SPIONs (SPIONs@APTS)

Synthesized SPIONs were functionalized by (3-aminopropyl) trimethoxysilane (APTS) to have peripheral amino groups [78–80]. Briefly, 1g of SPIONs were dispersed in 300 ml EtOH with probe sonication for 1 h. Then 6 ml of APTS was added to the EtOH solution. The solution was sonicated for another 1 h. The resulting product SPIONs@APTS were precipitated using a strong neodymium N52 magnet and then the reaction mixture was decanted. The product was washed 3 times by dispersing in 300 ml EtOH with probe sonication, followed by magnet decantation. SPIONs@APTS were dried under vacuum on a rotary evaporator. Energy dispersive X-ray spectroscopy (EDS) and FTIR spectroscopy

were used to characterized the product. Size and zeta potential were measured by Beckman Coulter Delsa Nano instrument.

2.3.2. Carboxylation of amine functionalized SPIONs (SPIONs@COOH)

Succinic anhydride was used to carboxylate the amine groups of SPIONs@APTS according to previously reported study [81]. Briefly, 100 mg of SPIONs@APTS were dispersed in 150 ml EtOH using probe sonication. Succinic anhydride (500 mg) was added to 150 ml of DMSO under vigorous stirring and then added to the SPIONs@APTS in EtOH solution. The reaction was stirred at RT for 24 h. The resulting product SPIONs@COOH were precipitated using a strong neodymium N52 magnet, followed by the decantation of the supernatant. The product SPIONs@COOH were washed 3 times by dispersing in 300 ml EtOH using probe sonication, followed by decantation, and were dried under vacuum on a rotary evaporator. The product was confirmed by FTIR spectroscopy, size, and zeta potential measurements.

2.3.3. Activation of SPIONs@COOH and fabrication of FA-PAMAM and SPIONs@COOH conjugate

Carboxyl groups of SPIONs@COOH were activated using carbodiimide reaction. In brief, 50 mg of SPIONs@COOH were dispersed in 100 ml DMSO using probe sonication for 1 h. Then, 490 mg EDC and 735 mg NHS were added to the solution. The reaction was left for 24 h under vigorous stirring. Activated SPIONs@COOH were conjugated with 100 mg PAMAM or 100 mg FA-PAMAM (dissolved in DMSO) to have SPIONs@PAMAM or SPIONs@FA-PAMAM. The final products SPIONs@PAMAM and SPIONs@FA-PAMAM were purified by

precipitation by a strong neodymium N52 magnet, followed by decantation of the supernatant. The products were washed 3 times by dispersing in 300 ml EtOH and followed by magnet decantation. The products were characterized by size and zeta potential measurements.

To quantify the amount of dendrimers conjugated to SPIONs, PAMAM dendrimers, and FA-PAMAM conjugates were labeled with Rhodamine B isothiocyanate according to previously reported method [82]. In short, PAMAM or FA-PAMAM conjugates were dispersed in 50 ml EtOH. Rhodamine B isothiocyanate was added to the EtOH dispersion. The amount of Rhodamine B isothiocyanate was calculated to have the ratio of Rhodamine B isothiocyanate to PAMAM or FA-PAMAM of 3:1. The reaction was stirred at RT for 1h, and followed by dialysis in 5L of DIW for 3 times with the molecular weight cut-off 3.5 kDa. Lyophilization was performed at the end of the dialysis to have the dry powder of Rhodamine B label PAMAM (RhoB-PAMAM) and Rhodamine B labeled FA-PAMAM (RhoB-FA-PAMAM). Fluorescence spectroscopy was employed to measure the fluorescence of the Rhodamine B labeled formulations (SPIONs@RhoB-PAMAM and SPIONs@RhoB-FA-PAMAM). The amounts of PAMAM and FA-PAMAM conjugated to SPIONs were calculated based on the linear equation of Rhodamine B fluorescence and Rho B-PAMAM or Rho B-FA-PAMAM concentrations.

2.3.4. Transmission electron microscopic analysis

The size of the synthesize SPIONs and the fabricated product SPIONs@PAMAM and SPIONs@FA-PAMAM were studied using transmission

electron microscopy. Samples were prepared according to a previous method [72]. Briefly, 4 µL of each sample (dispersion of 2 mg powder of the sample in 5 ml of DIW) was applied to a Formvar-coated, carbon-stabilized copper grid (400 mesh). The copper grid was air-dried and negatively stained with 5% aqueous uranyl acetate, and was allowed to dry. Samples were analyzed by JEOL Transmission electron microscope equipped with LaB6 filament gun (JEM 2010, Tokyo, Japan) at an accelerating voltage of 200 kV.

2.4. CDF encapsulation

Anticancer drug CDF was encapsulated in SPIONs@PAMAM and SPIONs@FA-PAMAM separately using equilibrium dialysis method as described earlier [72,83]. Briefly, CDF and SPIONs formulations were calculated to have CDF and dendrimer (PAMAM or FA-PAMAM) at the molar ratio of 50:1. Both CDF and SPIONs@PAMAM or SPIONs@FA-PAMAM were dissolved in the mixture of DMSO and phosphate buffered saline (PBS) pH 7.4 (ratio 4:6). The mixed solution was stirred in the dark at a low speed of 50 rpm for 72h at RT. The CDF encapsulated SPIONs@PAMAM-CDF and SPIONs@FA-PAMAM-CDF were precipitated using a strong neodymium N52 magnet. The supernatant was used for indirect drug loading method. After decantation, the formulations were washed by dispersing in 100 ml EtOH by vortexing, followed by magnet decantation. Dry products were obtained by drying under vacuum on a rotary evaporator.

The remaining CDF in the supernatant after drug loading was determined by High-performance liquid chromatography (HPLC) method using a C18 column with photodiode array detector (PDA) at 447 nm. For the remaining CDF

concentration determination, a standard curve of CDF was made by dissolving known amounts of CDF in DMSO and its successive dilutions in the mobile phase, followed by HPLC analysis at the absorbance of 447 nm. A known amount of the supernatant containing unloaded CDF was diluted in DMSO, followed by further dilution in the mobile phase and HPLC analysis at the absorbance of 447 nm. The amount of remaining CDF was calculated based on the CDF standard curve, and the percentage of CDF loaded in the formulations were calculated based on the subtraction of the initial amount of CDF and the remaining amount of CDF.

2.5. Fluorescence microscopy study

Fluorescence microscopic study was performed in SKOV3 cells to compare the targeting ability of SPIONs@FA-PAMAM and SPIONs@PAMAM. In brief, SKOV3 cells were seeded in a four-well chamber slide (5×10^4 cells in each well) and incubated at 37ºC in a 5% CO_2 air humidified atmosphere for 24 h. The medium was removed and Rhodamine B labeled formulations (SPIONs@PAMAM-Rho and SPIONs@FA-PAMAM-Rho) were added and incubated for 6 h. The formulation containing medium was removed, and cells were washed for 3 times with cold PBS (pH 7.4), and fixed with 3% formaldehyde in the PBS pH 7.4 at RT for 10 min. Samples were analyzed qualitatively using a fluorescent microscope (Leica, Germany) [84].

2.6. T_2 relaxivity and *in vitro* relaxometry and imaging studies

2.6.1. T_2 relaxivity studies of SPIONs, SPIONs@PAMAM, and SPIONs@FA-PAMAM

T_2 relaxometry was performed using a 7.0 T Bruker ClinScan system. The instrumental parameters wecre set as follows: a 7.0 T magnetic field strength, pixel spacing at 0.297/0.297, repetition time 2000 ms, echo time 11 ms, and slice thickness of 2 mm. Synthesized SPIONs and their modification SPIONs@PAMAM and SPIONs@FA-PAMAM were analyzed at different iron concentrations 10, 20, 40, 60, 80, and 100 µg/ml. The T_2 relaxivity was calculated from the linear slope of the inverse T_2 ($1/T_2$) relaxation time according to the iron concentration.

2.6.2. *In vitro* MR relaxometry and imaging

5 x 10^5 HeLa and SKOV3 cells were incubated with both the non-targeted formulation SPIONs@PAMAM and the targeted formulation SPIONs@FA-PAMAM at iron concentrations of 10,20,40, and 80 µg/ml for 30 min at 4^{o}C according to the previously reported method [59]. In short, 5 x 10^5 HeLa and SKOV3 cells were trypsinized and suspended in cold PBS (in an ice bath) and incubated with the formulations. After 30 min incubation, cells were centrifuged down at 800 rpm for 3 min to form a pellet. Cells were washed 3 times with cold PBS to remove free particles. Final pellets were resuspended in cold PBS and used for MR imaging. A phantom was constructed consisting of all of the sample vials. The instrumental parameters were set a 7.0 T magnetic field strength, pixel spacing at 0.297/0.297, repetition time 2000 ms, echo time 11 ms, and slice thickness of 2 mm.

2.7. *In vitro* cytotoxicity study

The *in vitro* cytotoxicity of free CDF, SPIONs@PAMAM-CDF, and SPIONs@FA-PAMAM-CDF formulations were evaluated by MTT assay on HeLa and SKOV3 cell lines. In brief, HeLa and SKOV3 cells were seeded in 96 well-plates with an average of 3000 cells in each well. After 24 h incubation at 37ºC in a 5% CO_2 air humidified atmosphere, cells were treated with various formulations with a concentration range from 0.25 µM to 5 µM. Treated cells were incubated for 72 h at 37ºC followed by addition of MTT solution (1mg/ ml) and further incubation at 37ºC for 3h. Then, the media was replaced by DMSO (100 µl in each well). The absorbance was measured at 590 nm using a high-performance multi-mode plate reader Synergy 2 (BioTek). The percentage of viable cells was determined by comparing the absorbance with appropriate controls [7,13].

2.8. Folate receptor blocking assay

The folate receptor blocking assay was performed to understand the mechanism by which the targeting SPIONs@FA-PAMAM-CDF internalize HeLa and SKOV3 cells via folate receptor mediated endocytosis. This assay is based on the principle of the initial blockade of folate receptors of HeLa and SKOV3 by adding an excess amount of free FA (1 mM) [72], followed by treatment with formulations (CDF, SPIONs@PAMAM-CDF, and SPIONs@FA-PAMAM-CDF). The cell viability of HeLa and SKOV3 were determined by MTT assay after 72 h incubation at 37ºC. This assay is performed according to the previously reported protocol [85]. In short, HeLa and SKOV3 cells were seeded in 96 well-plates for 24 h, followed by addition of 100 µl of 1mM FA in each well and incubation at 37ºC

for 3 h. Then, cells were washed twice with PBS (pH 7.4), followed by media and addition of formulations. After 72 h incubation at 37°C, MTT assay was performed to determine the cell viability as stated in the previous section.

2.9. Apoptosis assay by flow cytometry

Apoptosis assay was performed on HeLa cell line according to our previous study [72]. In brief, HeLa cells were cultured in 6-well plates at $5x10^4$ cells in each well and incubated for 24 h at 37°C under 5% CO_2, followed the treatment of plain CDF, SPIONs@PAMAM-CDF, and SPIONs@FA-PAMAM-CDF to induce apoptosis. The concentration of CDF, SPIONs@PAMAM-CDF and SPIONs@FA-PAMAM-CDF were chosen based on the IC_{50} value of CDF on HeLa cells from the *in vitro* cytotoxicity assay. After 72h incubation, cells were collected and the sample was prepared according to the protocol for Guava Nexin Annexin V assay (EMD Millipore, USA). In short, media and trypsinized treated cells were collected in 15 ml tubes and centrifuged at 300 x g for 7 min. Cell pellets were dispersed in PBS pH 7.4 with 1% FBS to have the number of cells in the range of $2 \times 10^5 - 1 \times 10^6$ cells/mL. Then 100 µL of cell dispersion of each sample was added 100 µL of the Guava Nexin Reagent and was incubated for 20 min at RT in the dark. The samples were analyzed by Guava Easycyte flow cytometer (EMD Millipore, USA).

2.10. Western blot

Western blot analysis was performed to determine the level expression of Phosphatase and tensin homolog PTEN and Nuclear factor kappa B (NF-κB) in HeLa cell line using reported method [86]. Briefly, HeLa cells were treated with different formulations as well as free CDF and lysed. The protein concentration

was determined by the Bio-Rad Protein Assay (Bio-Rad kit). Lysates were electrophoresed by SDS-PAGE and the proteins were transferred onto the nitrocellulose blotting membrane, followed by blocking with 5% BSA in TBST buffer at RT for 1h. Primary PTEN or NF-κB antibodies were added and incubated overnight at 4^{o}C, subsequently washed and incubated with compatible secondary antibodies. The protein bands were visualized by incubation with chemiluminescent substrate (Thermos scientific) at room temperature for 2 min, followed by chemiluminescent detection using a digital imaging system ImageQuant LAS 4000 (GE Healthcare Bio-Sciences AB, Sweden).

CHAPTER 3 RESULTS

A vast majority of cancer cells are known to have a high expression of folate receptors, while normal tissues and organs have very limited expression of folate receptors [87]. Many studies have shown an enhance in anticancer activity employing folic acid decorated nanocarriers in different cancer types such as ovarian, lung, cervical, breast, kidney, colorectal, epithelial and brain cancers [85,88–90]. CDF has been shown a high anticancer activity against various types of cancers as well as overcome drug resistance [11,86]. However, extremely low aqueous solubility of CDF makes its systemic administration problematic. Our previous study suggested that PAMAM dendrimer conjugated with folic acid could improve the aqueous solubility of CDF dramatically and gave the active targeting with an enhanced anticancer activity due to the folate receptor mediated endocytosis [72]. In addition, many studies reported the potential usage in biomedical imaging of PAMAM dendrimers when fabricated with magnetic iron oxide nanoparticles [59,78,91–93]. Based on these information, the goal of this present work was to design a theranostic nanoparticles consisting of FA-PAMAM conjugate as the outer shell and iron oxide nanoparticles as the inner core loaded with CDF which could be used in both cancer imaging and therapy for multiple cancers.

3.1. SPIONs synthesis and characterization

The magnetic iron oxide nanoparticles SPIONs were synthesized by controlled co-precipitation of Fe^{2+} and Fe^{3+} ions according to previously reported method [77,94,95]. The synthesized SPIONs were confirmed by FTIR

spectroscopy. The presence of Fe_3O_4 core was identified by the strong stretching absorption band between 408 and 673 cm^{-1} corresponding to the Fe-O bond of the particles (Fig. 3a) [78]. Dynamic light scattering technique measurement showed a hydrodynamic size of 78.8 nm (PDI 0.177) and a zeta potential at – 59.73 mV (Fig. 3d).

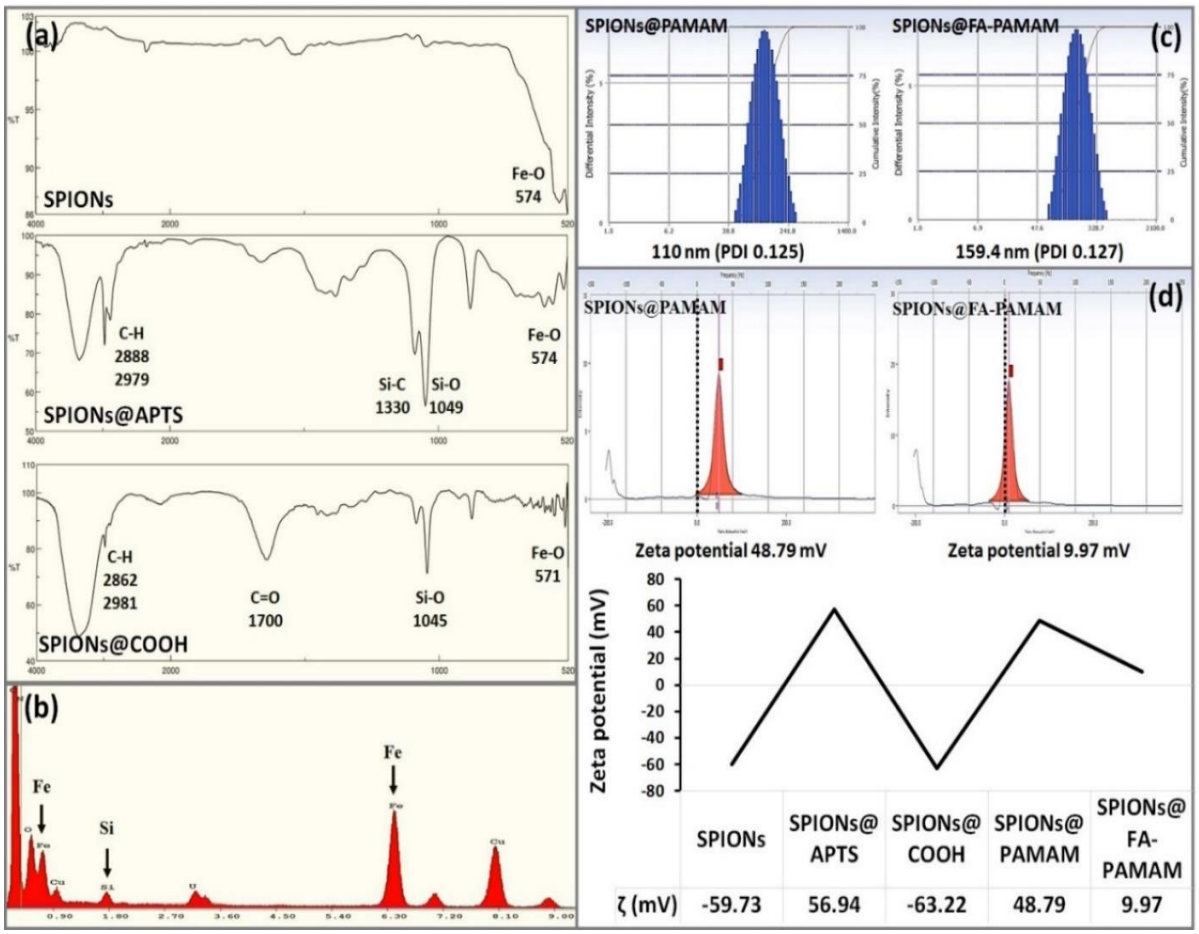

Figure 3. (a) FTIR spectra of SPIONs, SPIONs@APTS, and SPIONs@COOH; (b) Energy dispersive X-ray spectroscopy (EDS) analysis of SPIONs@APTS; (c) Hydrodynamic size of the fabricated nanoparticles SPIONs@PAMAM and SPIONs@FA-PAMAM; and (d) Zeta potential measurement of each step of the fabrication process are shown.

3.2. FA-PAMAM decorated SPIONs fabrication and characterization

3.2.1. Amine functionalized SPIONs (SPIONs@APTS)

The sonication time was optimized according to previous reported method [78]. Sonication of the synthesized SPIONs before modification with APTS improved the magnetic properties and size distribution of the particles. After aminosilane modification of the SPIONs, the achieved product SPIONs@APTS could be dispersed back in DIW to form a stable dispersion with a hydrodynamic size of 95.9 nm (PDI 0.113). SPIONs@APTS showed a zeta potential of 56.94 mV confirming the presence of the positively charged amine groups of APTS (Fig 3d). Energy-dispersive X-ray spectroscopy (EDX) spectrum showed the unique peak of Si further confirmed the successful coating of the aminosilane APTS on the surface of SPIONs (Fig 3b). FTIR spectrum confirmed the presence of APTS on the surface of SPIONs with the characteristic peaks of C-H at 2888, 2979 cm^{-1}, Si-C at 1330 cm^{-1}, Si-O at 1049 cm^{-1}, and Fe-O at 574 cm^{-1} (Fig. 3a).

3.2.2. Carboxylation of amine functionalized SPIONs (SPIONs@COOH)

The carboxylation of primary amine groups on the surface of SPIONs@APTS was confirmed by the change in zeta potential from a positive charge of 56.94 mV (of the amine groups) to a negative charge of -63.22 mV (of the carboxyl groups) (Fig 3d). FTIR spectrum of SPIONs@COOH showed the characteristic peaks of C-H bond at 2981 cm^{-1} and 2862 cm^{-1}, Si-O bond at 1045cm^{-1}, Fe-O bond at 571 cm^{-1}, and the C=O stretching at 1700 cm^{-1} (Fig. 3a). SPIONs@COOH had a hydrodynamic size of 96.2 nm (PDI 0.246).

3.2.3. Activation of SPIONs@COOH and fabrication of FA-PAMAM and SPIONs@COOH conjugate

Zeta potential was used to confirmed the conjugation of PAMAM and FA-PAMAM to the activated SPIONs@COOH. Before conjugation, SPIONs@COOH had the zeta potential of -63.22 mV. After the conjugation, the zeta potential values were changed to 48.79 mV and 9.97 mV in case of SPIONs@PAMAM and SPIONs@FA-PAMAM, respectively (Fig. 3d). Dynamic light scattering showed an average size of 110.1 nm (PDI 0.125) and 159.4 nm (PDI 0.127) of SPIONs@PAMAM and SPIONs@FA-PAMAM, respectively (Fig 3c). Fluorescence spectroscopy measurement showed an average of 20.37% (wt/wt) of PAMAM in SPIONs@PAMAM, and 27.61% (wt/wt) of FA-PAMAM conjugates in SPIONs@FA-PAMAM structure.

3.2.4. Transmission electron microscopic analysis

To further determine the size of the nanoformulations, electron microscopic analysis of the synthesized SPIONs, and the carrier SPIONs@PAMAM and SPIONs@FA-PAMAM was performed. TEM images showed that the morphology of the fabricated SPIONs was remained the same as the unmodified SPIONs. TEM data showed that the inner SPIONs core had the average size of 11 nm confirming the nano-metric size of the formulations (Fig. 4).

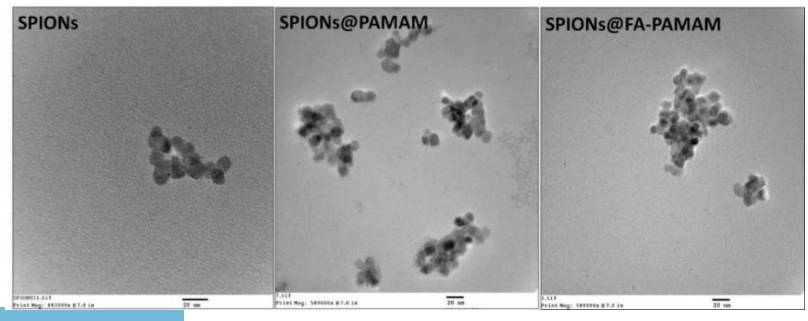

Figure 4. Transmission electron microscopic images of SPIONs, SPIONs@PAMAM and SPIONs@FA-PAMAM show the morphology of the fabricated nanoparticles.

3.3. CDF drug loading in nanoparticles

The CDF drug loading was studied based on the indirect method. The remaining of CDF in the supernatant after drug loading was measured by HPLC method. A calibration curve of CDF was developed from 10 µg/ml to 250 µg/ml with the R^2 value of 0.99. The HPLC method was validated for its accuracy and precision and was used to determine the CDF concentration. The loading of CDF in SPIONs@PAMAM and SPIONs@FA-PAMAM was 12.37% (wt/wt) and 9.81% (wt/wt), respectively.

3.4. Fluorescence microscopy study

SKOV3 cells were selected for *in vitro* fluorescence microscopic study based on the results of *in vitro* cytotoxicity assay and receptor blocking assay to compare the level of cellular internalization of the non-targeted formulation SPIONs@PAMAM-CDF and the targeted formulation SPIONs@FA-PAMAM-CDF. In this cell uptake studies, SKOV3 cells were incubated with Rhodamine B (having red fluorescence) labeled nanoformulations and analyzed after 6 hours of incubation at 37ºC in the dark. As shown in figure 5, SKOV3 cells treated with both of the non-targeted and the targeted formulations showed apparent fluorescence. As compared to the non-targeted formulation, there was a significantly higher fluorescence in cells treated with targeted formulations.

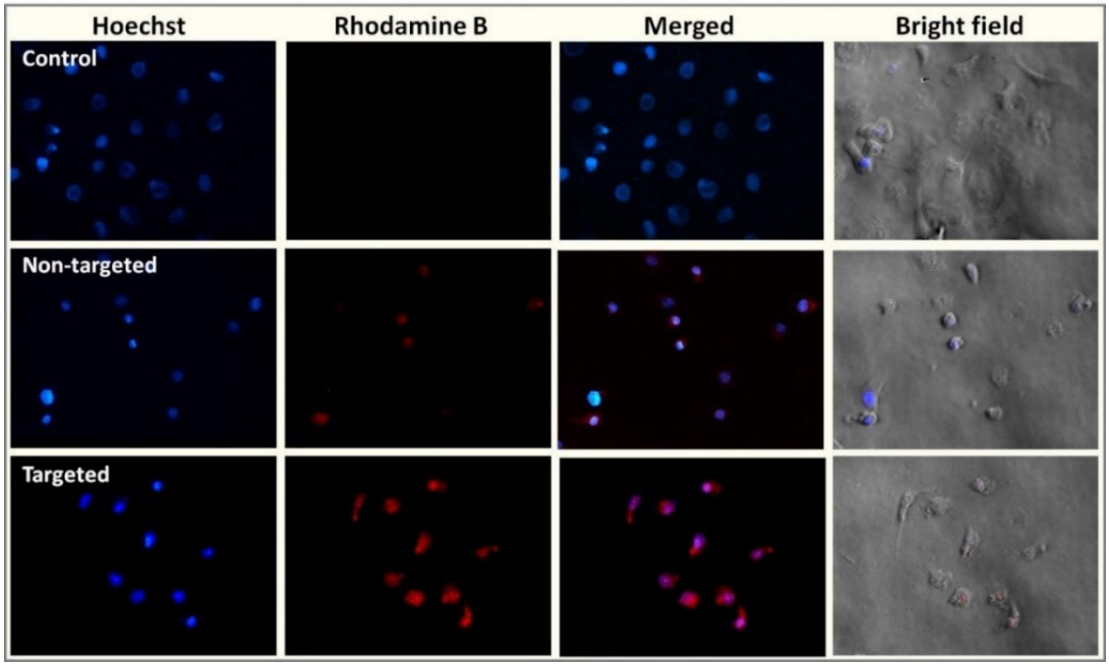

Figure 5. Fluorescence microscopic images (40X) of SKOV3 cells incubated with nuclear stain Hoechst (blue fluorescence) and Rhodamine B (red fluorescence) labeled non-targeted SPIONs@PAMAM and targeted formulations SPIONs@FA-PAMAM at 6 h are shown.

3.5. T2 relaxivity and in vitro relaxometry and imaging studies

3.5.1. T_2 relaxivity studies of SPIONs, SPIONs@PAMAM and SPIONs@FA-PAMAM

T_2 relaxivity studies were performed to examine the magnetic behavior of the synthesized SPIONs and the nano-carrier SPIONs@PAMAM and SPIONs@FA-PAMAM in their biomedical application in MR imaging. The potential of the fabricated magnetic nanoparticles SPIONs@PAMAM and SPIONs@FA-PAMAM to be used as T_2-based contrast agent for MR imaging was evaluated using the measured transverse relaxation time (T_2) of SPIONs@PAMAM and SPIONs@FA-PAMAM as compared to SPIONs. The T_2 values were used to calculate the transverse relaxivity rate (r_2) per µg/ml of iron, which showed the

efficiency of the fabricated nanoparticles as a MR contrast agent. From figure 6a, there was a significant decrease in the signal intensity of the T_2-weighted MR images with the increase of iron concentration in both of the non-targeted SPIONs@PAMAM and the targeted SPIONs@FA-PAMAM nanoparticles as compared to the control PBS. Pseudo-color MR images showed a decrease in signal intensity for the fabricated nanoparticles from red (high intensity) to purple (low intensity). The T_2 relaxation rate ($1/T_2$) increased linearly with the iron concentration (μg/ml) in both cases of the non-targeted SPIONs@PAMAM and the targeted SPIONs@FA-PAMAM nanoparticles. The slope values (r_2) were calculated to be 1.92 $(\mu g/ml)^{-1}s^{-1}$ and 1.81$(\mu g/ml)^{-1}s^{-1}$ in case of SPIONs@PAMAM and SPIONs@FA-PAMAM, respectively. Unmodified SPIONs had the slope value (r_2) of 2.01 $(\mu g/ml)^{-1}s^{-1}$. The results suggested that both of the non-targeted nanoparticle SPIONs@PAMAM and the targeted nanoparticle SPIONs@FA-PAMAM could be used as T_2-shortening agents.

3.5.2. *In vitro* MR relaxometry and imaging studies

In vitro MR relaxometry and Imaging studies were performed to examine the effect of the targeting ability of folate-based nanoparticle SPIONs@FA-PAMAM in MR imaging. To study the effect of SPIONs@PAMAM and SPIONs@FA-PAMAM on SKOV3 and HeLa cells, we measured the T_2 of SKOV3 and HeLa cells after incubation with different concentration of SPIONs@PAMAM and SPIONs@FA-PAMAM for 30 min. There was a significant decrease in signal intensity in SKOV3 and HeLa cells when incubated with the targeted nanoparticle SPIONs@FA-PAMAM. In contrast, non-targeted nanoparticle SPIONs@PAMAM

showed a very little decrease in the signal intensity in both SKOV3 and HeLa cells. In the T_2-weighted MR images, targeted formulation SPIONs@FA-PAMAM at the iron concentration of 80 µg/ml decreased the MR signal intensity to 45.6% in SKOV3 and 28% in HeLa, as compared to 100% of PBS control. However, non-targeted nanoparticle SPIONs@PAMAM at the iron concentration of 80 µg/ml showed a lower decrease in MR signal intensity with 87% in SKOV3 and in 71.4% HeLa, as compared to 100% of control PBS (Fig 6b).

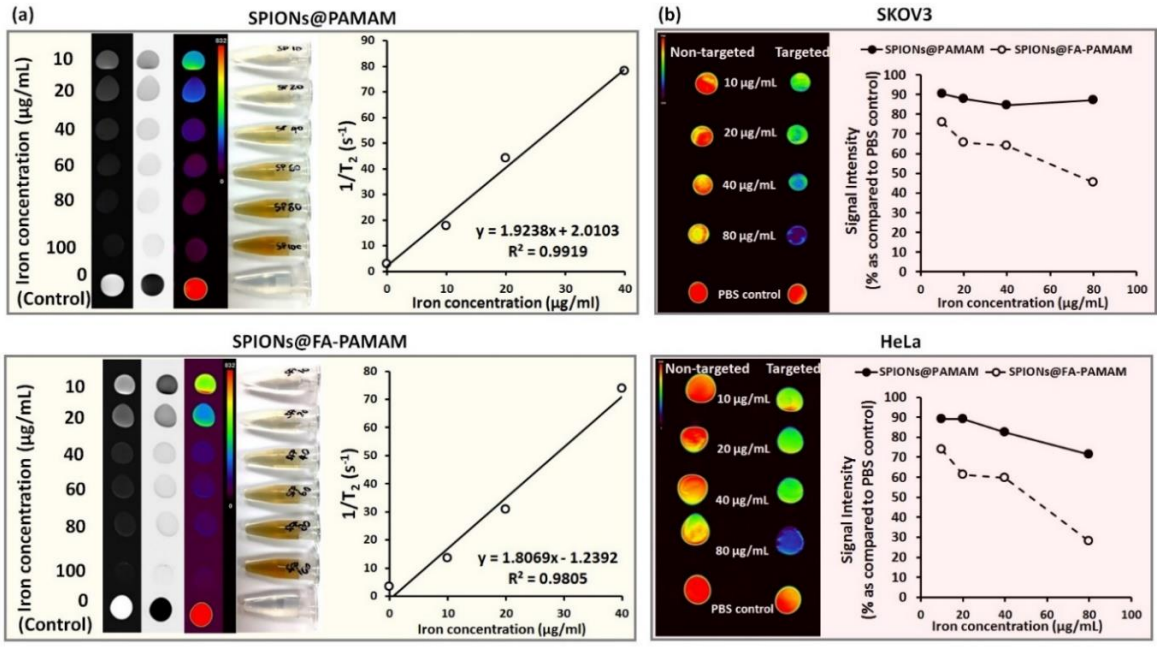

Figure 6. (a) T_2-weighted MR images of the aqueous dispersion of SPIONs@PAMAM and SPIONs@FA-PAMAM with the T_2 relaxation rate ($1/T_2$) as a function of iron concentration indicating the ability of the fabricated nanoparticles to enhance the contrast in MR images; (b) MR images of SKOV3 and HeLa cell pellets after 30 min incubation with the non-targeted SPIONs@PAMAM and the targeted SPIONs@FA-PAMAM nanoparticles (with the color change from red to purple indicating the gradual decrease of MR signal intensity). The percentage of signal intensity compared to cells in PBS was plotted as a function of iron concentration indicating the faster internalization with a higher decrease in MR signal intensity of the targeted SPIONs@FA-PAMAM.

3.6. *In vitro* cytotoxicity study

In vitro cytotoxicity of the CDF loaded nanoformulations was examined in 2 cell lines [SKOV3 (human ovarian carcinoma cell line), HeLa cells (human cervical cancer cells)] with a broad range of CDF concentrations (0.25 µM - 5 µM). Plain targeted carrier (SPIONs@FA-PAMAM) showed negligible cytotoxicity with cell viability more than 90% confirming the safety of the targeted carrier. The anticancer activity of the nanoformulations (non-targeted formulation SPIONs@PAMAM-CDF and targeted formulation SPIONs@FA-PAMAM-CDF) was studied and compared with free drug CDF. The results showed a dose-dependent cell killing for both SPIONs@PAMAM-CDF and SPIONs@FA-PAMAM-CDF. The outcome of the study revealed an IC_{50} (half maximal inhibitory concentration) of 0.45 µM, 0.78 µM, and 1.79 µM for free CDF, SPIONs@FA-PAMAM-CDF, and SPIONs@PAMAM-CDF, respectively in SKOV3 cells. The noticeably lower IC_{50} of the targeted SPIONs@FA-PAMAM-CDF as compared to the non-targeted SPIONs@PAMAM-CDF was probably due to the folate receptor-specific targeting of SPIONs@FA-PAMAM-CDF. The same pattern was also observed in HeLa cells with the IC_{50} of 0.66 µM, 0.87 µM, and 1.98 µM for free CDF, SPIONs@FA-PAMAM-CDF, and SPIONs@PAMAM-CDF, respectively (Fig. 7a).

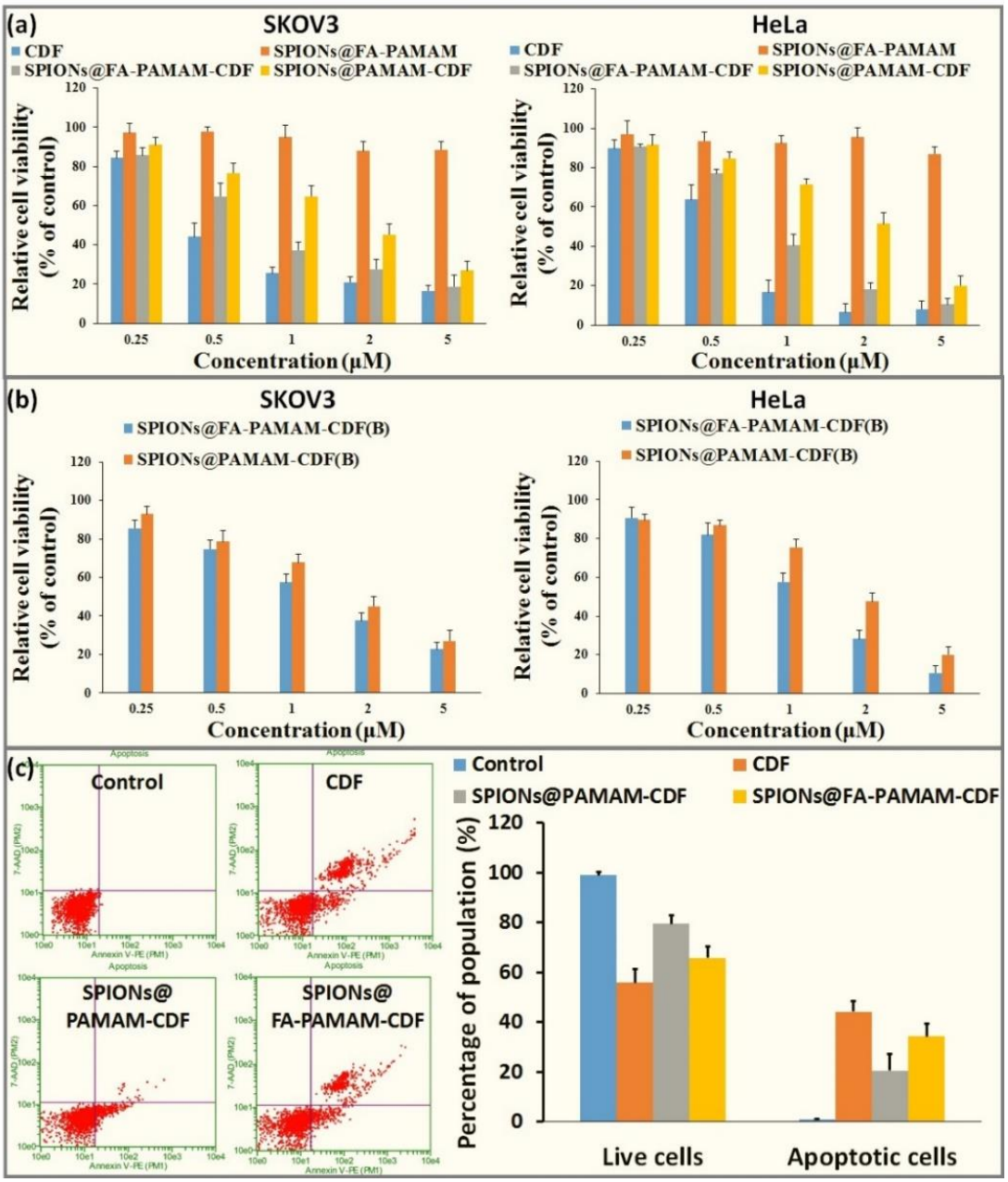

Figure 7. (a) *In vitro* cytotoxicity assay showing percentage of cell viability observed at 72 h after treating SKOV3 and HeLa cells with various formulations are shown (n=8); (b) MTT assay observed at 72 h after folate receptor blocking and treating of SKOV3 and HeLa cells with SPIONs@PAMAM-CDF and SPIONs@FA-PAMAM-CDF are shown (n=8); (c) Induction of apoptosis in HeLa cells when treated with CDF, SPIONs@PAMAM-CDF, and SPIONs@FA-PAMAM-CDF as evaluated by Annexin V/7-AAD dual staining. An increased percentage of the apoptotic cell population was noted when cells were treated with targeted formulation (SPIONs@FA-PAMAM-CDF) as compared to the non-targeted formulation (SPIONs@PAMAM-CDF), suggesting the better killing activity of the targeted formulation SPIONs@FA-PAMAM-CDF.

3.7. Folate receptor blocking assay

Folate receptor blocking assay was performed to examine the fate of the folate-based targeting formulation. SKOV3 and HeLa cells with high expression of folate receptors were treated with an excess amount of FA (1 mM) to overwhelm the folate receptor binding domains on the cell membrane, followed by the treatment with the nanoformulations [73–76,96]. *In vitro* cytotoxicity MTT assay was used to determine the change in the cell viability in SKOV3 and HeLa treated with the formulations after blocking the folate receptors. It was observed that before blockade of folate receptors, the IC_{50} values on SKOV3 were 0.80 μM and 1.81 μM for the targeted SPIONs@FA-PAMAM-CDF and the non-targeted SPIONs@PAMAM-CDF, respectively. After the blockade of folate receptors, the IC_{50} value of the targeted SPIONs@FA-PAMAM-CDF was increased to 1.36 μM. However, there was not a significant change in the IC_{50} of the non-targeted SPIONs@PAMAM-CDF (1.82 μM). The same outcome was observed in HeLa cells with the IC_{50} of 0.85 μM and 2 μM for SPIONs@FA-PAMAM-CDF and SPIONs@PAMAM-CDF, respectively before the folate receptor blockade. After blocking folate receptors, the IC_{50} values were found to be 1.26 μM and 1.94 μM for SPIONs@FA-PAMAM-CDF and SPIONs@PAMAM-CDF, respectively. The results suggested a decrease in anticancer activity of the targeted formulation SPIONs@FA-PAMAM-CDF in SKOV3 cells when folate receptors are blocked (Fig. 7b).

3.8. Apoptosis assay

HeLa cells were selected for this apoptosis assay. Apoptosis induction in HeLa cells of free CDF and the CDF loaded formulations was determined by flow cytometry with Annexin V/7-AAD dual staining. The percentage of Annexin V^-/7-AAD^- (R5), Annexin V^+/7-AAD^- (R6) and Annexin V^-/7-AAD^+ (R4) and Annexin V^-/7-AAD^+ (R3) were used to determine the number of live cells, early apoptotic, late apoptotic and necrotic cells. Apoptosis assay revealed a higher percentage of apoptotic and necrotic HeLa cells (34.2 ± 3.2 %) after treatment with the targeted formulation SPIONs@FA-PAMAM-CDF. Non-targeted formulation showed a lower number of apoptotic and necrotic cells at 20.5 ± 2.7 % of the cell population. The results suggested a higher apoptosis induction ability of the targeted formulation SPIONs@FA-PAMAM-CDF as compared to the non-targeted formulation SPIONs@PAMAM-CDF (Fig. 7c). The results were consistent with higher anticancer activity of the targeted formulation SPIONs@FA-PAMAM-CDF in *in vitro* cytotoxicity assay using MTT with higher cellular uptake in fluorescence microscopic studies and *in vitro* relaxometry and imaging studies.

3.9. Western blot

Western blot was performed to examine the level expression of PTEN and NF-κB in HeLa cells after treatment with the nanoformulations. In case of NF-κB, control HeLa cells without treatment showed a higher expression of NF-κB as compared to HeLa cells treated with plain CDF and the nanoformulations. Targeted formulation SPIONs@FA-PAMAM-CDF showed a slightly better downregulation of NF-κB (76.4 ± 4.6 % as of control) as compared to the non-

targeted formulation SPIONs@PAMAM-CDF (83.6 ± 8.2 % as of control). In case of PTEN expression, the control HeLa cells without treatment showed a significantly low expression of PTEN. However, after treatment with plain CDF and nanoformulations, PTEN expression was elevated. Noticeably, in comparison to control, HeLa cells treated with the targeted formulation SPIONs@FA-PAMAM-CDF showed the highest upregulation of PTEN expression (319.9 ± 27.1 %) as compared to free CDF (158.9 ± 13.5 %) and the non-targeted formulation SPIONs@PAMAM-CDF (214.2 ± 10.9%) (Fig. 8).

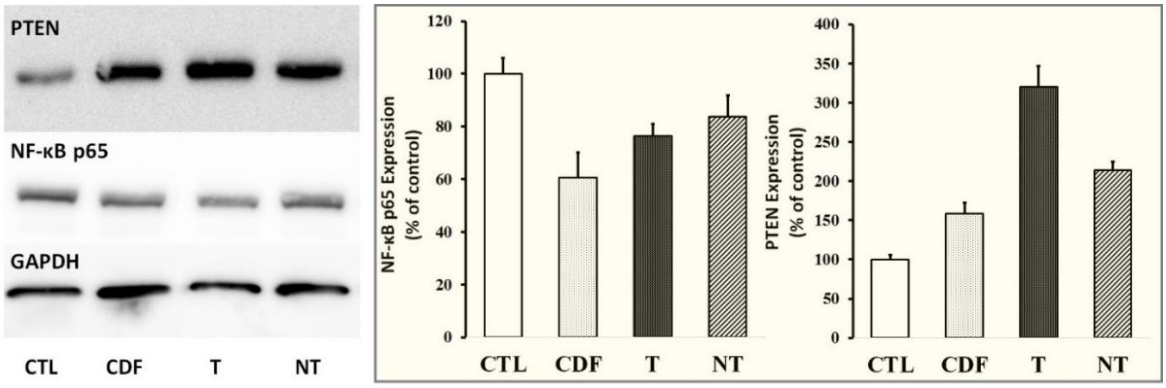

Figure 8. Western blot analysis showing PTEN and NF-κB expression in HeLa cells in control without treatment (CTL), and cells treated with CDF, targeted formulation SPIONs@FA-PAMAM-CDF (T) and non-targeted formulation SPIONs@PAMAM-CDF (NT), (GAPDH expression was used as the protein loading control).

CHAPTER 4 DISCUSSION

The bleak prognosis for patients diagnosed with metastatic cancer along with the high costs of treating cancer in its advanced stages are urging for a better predictive and preventative method [97]. With the advantages of noninvasive MR imaging with superb spatial resolution, targeting MRI contrast agents are believed to be critical tools which can fully benefit from this new technique [98,99]. The targeting ability of MRI contrast agents depends strongly on their ability to carry specific molecular markers for tumor recognition. As a result, the tumor can be visualized and diagnosed earlier accurately leading to an effective treatment, and ultimately improving patient survival [37,98]. In this regards, PAMAM dendrimers with the ability to conjugate targeting ligands through numerous peripheral reactive amine groups have been studied recently for surface modification of iron oxide nanoparticles for targeting MRI [78,100,101]. In terms of targeting ligands, folic acid recently has received considerable attention as a targeting ligand to target folate receptors overexpressed on numerous types of tumors [89,90,96,102–106]. PAMAM dendrimers conjugated folic acid can take advantage of the favorable binding of targeting ligand folic acid to folate receptors on tumor cells to enhance the cellular uptake via folate receptor mediated endocytosis. Many studies have shown that iron oxide nanoparticles decorated with folate-based PAMMA dendrimer could achieve MRI targeting with higher cellular internalization in cancer cells with a higher contrast in T_2-weighted MR images [59,71,78]. However, in most of the studies, the ability of PAMAM dendrimers in drug delivery was not fully examined.

The poor aqueous solubility of several potent anticancer compounds could be a major issue and deciding factor in realizing its translation potential from the bench to the bedside. The non-specific distribution of chemotherapeutic agents in the systemic circulation gives the conventional chemotherapy a low therapeutic index and severe side effects which cause the treatment to be ineffective and lead to the recurrence of tumor after initial treatment. Recently, CDF has been shown to be a very potent anticancer compound with the ability to treat different types of cancers [12,13,72]. However, low solubility profile of CDF makes its systemic administration problematic. In this regard, PAMAM dendrimers have revealed promising potentials. Our earlier reported study suggested that folate-decorated PAMAM dendrimers could encapsulate CDF in their hydrophobic cavities for aqueous solubility enhancement and deliver CDF specifically to the tumor site with minimizing adverse side effects [72]. The aim of this study was to design a theranostic carrier consisting of iron oxide nanoparticles with folate-based PAMAM dendrimers for active targeting MR imaging and anticancer drug delivery. As a result, the targeted nanoparticles SPIONs@FA-PAMAM can enhance the aqueous solubility of CDF and deliver it specifically to cancer cells with a higher contrast in T_2-weight MR images.

The synthesis of SPIONs was confirmed by FTIR spectrum with the characteristic peak of Fe-O at 574 cm^{-1}. The synthesized SPIONs could be dispersed back in DIW or EtOH to form a stable dispersion with a hydrodynamic size of 78.8 nm (PDI 0.177) and a zeta potential of -59.73 mV. TEM images of SPIONs showing an average size at 10.5 ± 1 nm further reconfirmed the success

of the synthesis. Surface modification of SPIONs was confirmed by zeta potential with a change from an initial zeta potential of -59.73 mV of SPIONs to 56.94 mV of SPIONs@APTS, and -63.22 mV of SPIONs@COOH (Fig 3d). In EDX analysis of SPIONs@APTS, the atomic ratio of Fe/Si was shown to be 17.55/1 (Fig. 3b). The mathematic calculation was used to estimate the number of silanes per gram particles according to the reported method [77]. From TEM images, synthesized SPIONs were shown to have an average diameter (r_{SPIONs}) of 5.5 nm; therefore, the surface area (SA_{SPIONs}) of one particle is 380 nm^2 ($SA_{SPIONs} = 4\pi r_{SPIONs}^2$). One silane is known to cover an approximately 0.4 nm^2 of the particle's surface area, so we have an average of 950 silanes covered the surface of one SPION [77]. With the atomic ratio 17.55/1 of Fe/Si in SPIONs@APTS from EDX analysis, it is estimated that 950 silanes would cover one particle with an average of 16,672.5 iron atoms. Therefore, 1 g of SPIONs would have an average of 0.099 g of APTS coating, theoretically.

PAMAM and FA-PAMAM conjugation was confirmed by a change in zeta potential. After conjugation, SPIONs@PAMAM and SPIONs@FA-PAMAM had a zeta potential of 48.79 mV and 9.97 mV, respectively (Fig. 3d). FA conjugation helped the targeted carrier SPIONs@FA-PAMAM reduce the highly positive charge, which is known to be associated with the toxicity of PAMAM dendrimers [16]. The morphology of nanoparticles could be affected by several factors including the fabrication and reaction involved. The shape and size of nanoparticles could have a high impact on their biodistribution, clearance, and biocompatibility [107]. TEM images suggested that the morphology of the particles

remained unchanged after the fabrication. Dynamic light scattering measurement showed that both of the non-targeted and targeted formulations were in the nano-sized range with an average hydrodynamic size of 110.1 nm (PDI 0.125) and 159.4 nm (PDI 0.127) of SPIONs@PAMAM and SPIONs@FA-PAMAM, respectively (Fig 3c). A higher value in hydrodynamic size of SPIONs@FA-PAMAM could be attributed to the presence of FA resulting in a low positive charge of the particles. Drug loading studies showed a little higher in CDF encapsulation in SPIONs@FA-PAMAM-CDF as compared to SPIONs@PAMAM-CDF. The presence of FA might be responsible for a higher drug loading with a shielding effect outside the hydrophobic cavities; thus, a higher amount of CDF was encapsulated inside the hydrophobic cavities.

Targeting ability of folate-decorated nanoformulations was examined in fluorescence microscopic study on SKOV3 cell line. SKOV3 cells treated with Rhodamine B labeled targeted formulation SPIONs@FA-PAMAM-CDF showed a significantly higher red fluorescence intensity of Rhodamine B dye as compared to the Rhodamine B labeled non-targeted formulation SPIONs@PAMAM. The fluorescence microscopic images were taken after only 6 h incubation of SKOV3 cells with the Rhodamine B labeled formulations, which proved the ability of the targeted formulation to internalize the cells within such a short time frame [Fig 5].

The magnetic behavior of the non-targeted SPIONs@PAMAM and the targeted SPIONs@FA-PAMAM was examined in the T_2 relaxivity studies to test their ability to enhance the contrast in MR images [Fig 6]. The T_2 relaxation rate ($1/T_2$) as a function of the iron concentration (from 10 µg/ml to 40 µg/ml) of both of

the carriers showed that the relaxation rate increases linearly with the iron concentration with a slope (r_2) of 1.92 $(\mu g/ml)^{-1}s^{-1}$ and 1.81$(\mu g/ml)^{-1}s^{-1}$ for SPIONs@PAMAM and SPION@FA-PAMAM, respectively. The slightly lower r_2 of SPIONs@FA-PAMAM may be due to the presence of FA on the periphery of the particles, which shields water molecules from accessing the surface of SPIONs. The results suggested that SPIONs@PAMAM and SPIONs@FA-PAMAM could be used as T_2-shortening agents which helped enhance the contrast in the MR images. To study the effect of the non-targeted SPIONs@PAMAM and the targeted SPIONs@FA-PAMAM on the MR images of SKOV3 and HeLa cells, T_2 of SKOV3 and HeLa cells was measured after 30 min incubation with various concentrations of SPIONs@PAMAM and SPIONs@FA-PAMAM. The T_2 values of SKOV3 and HeLa cell pellets treated with SPIONs@FA-PAMAM particles decreased dramatically as a function of iron concentration. In contrast, there was a small decrease in the T_2 values of SKOV3 and HeLa cell pellets treated with the non-targeted SPIONs@PAMAM particles. In the T_2-weighted MR images (the color change from red to purple indicates a decrease in MR signal intensity) observed in SKOV3 and HeLa cells, targeted SPIONs@FA-PAMAM nanoparticles at 80 μg/ml reduced the signal intensity to 45.6% and 28% of the initial value (PBS control) in SKOV3 and HeLa cells, respectively; whereas non-targeted SPIONs@PAMAM nanoparticles at 80 μg/ml reduced the signal intensity to 87% and 71.4% of the initial value in SKOV3 and HeLa cells, respectively. The results suggested the targeted nanoparticles SPIONs@FA-PAMAM can specifically hamper the MR signal intensity through folate receptor mediated endocytosis. The

results are in accordance with the higher cellular internalization of the targeted nanoparticles in the fluorescence microscopic studies.

The anticancer activity of the CDF loaded nanoformulations was examined using the *in vitro* cytotoxicity assay on SKOV3 and Hela cells. The MTT assay results showed a high anticancer activity on SKOV3 and HeLa cells with both the formulations with relatively low IC_{50}. It should be noted that the targeted formulation SPIONs@FA-PAMAM-CDF showed a higher anticancer activity with lower IC_{50} as compared to the non-targeted formulation SPIONs@PAMAM-CDF when tested at a concentration range from 0.25 µM to 5 µM. IC_{50} values of SPIONs@FA-PAMAM-CDF were found to be 0.78 µM and 0.87 µM in SKOV3 and HeLa, which were lower by 2.29 fold and 2.27 fold as compared to the non-targeted SPIONs@PAMAM-CDF in SKOV3 and HeLa, respectively. The better anticancer activity of the targeted formulation could be attributed to the targeting effect of FA, which helped the formulations have a higher degree of cellular internalization via folate receptor mediated endocytosis. Fourth generation PAMAM dendrimers are known to be cytotoxic due to the highly positive charge of 64 amino groups on the periphery. FA conjugation gave the targeted formulation the ability to target folate receptors overexpressed on cancer cells, and also helped reduce the positive charge of the nanoconstruct. As a result, SPIONs@FA-PAMAM carrier showed a relatively safe profile on both SKOV3 and HeLa cells with more than 90% viable cells at all tested concentrations. The results proved that SPIONs@FA-PAMAM could be promising carriers for anticancer drug delivery (Fig 7a). The folate receptor assay was performed to evaluated the fate of the nanoformulations under

blocking the folate receptors. An increase in IC_{50} values of the targeted formulation SPIONs@FA-PAMAM-CDF in SKOV3 and HeLa cells after blocking folate receptors was observed. In contrast, IC_{50} values of the non-targeted formulation SPIONs@PAMAM-CDF did not show a significant change after the blocking of folate receptors. The results suggested that the higher activity of the targeted formulation SPIONs@FA-PAMAM-CDF was due to the active targeting ability of the folate-decorated nanoformulations. However, it should be noted that the IC_{50} value of SPIONs@PAMAM-CDF was still higher than SPIONs@FA-PAMAM-CDF in both SKOV3 and HeLa after the blocking the folate receptors (Fig 7b). The results suggested that the blocking of folate receptors on SKOV3 and HeLa cells could decrease the cellular uptake of the targeted formulation to a certain degree, and when the folate receptors are recycled, the folate receptor mediate endocytosis pathway was recovered and the targeting ability of SPIONs@FA-PAMAM was regained.

As a next step, apoptosis assay and western blot studies were performed to further examine the targeting ability of the targeted formulation SPIONs@FA-PAMAM-CDF in anticancer activity against HeLa cells. It should be noted that free CDF showed the highest percentage of apoptotic and necrotic cells. This could be explained by the small molecular weight and the highly lipophilic profile of CDF which gives CDF a high rate of internalization of passive diffusion. Apoptosis assay showed a higher percentage of apoptotic and necrotic cells in HeLa after treatment with the targeted formulation SPIONs@FA-PAMAM-CDF as compared to the non-targeted formulation SPIONs@PAMAM-CDF. A better apoptosis induction ability

of the targeted formulation SPIONs@FA-PAMAM-CDF could be explained by a higher cellular uptake of the formulation due to the targeting ability of FA to the folate receptors overexpressed on HeLa cells [Fig 7c]. The results from apoptosis assay were in accordance with higher anticancer activity of the targeted formulation with higher cellular uptake in fluorescence microscopic studies and *in vitro* T_2 relaxation studies.

Western blot studies were performed on HeLa cells to determine the expression levels of PTEN and NF-κB after treatment with the formulations. CDF is known to upregulate PTEN, which is a tumor suppressor gene with a key role in stem cell self-renewal [86]. PTEN can dephosphorylate phosphatidylinositol 3,4,5-triphosphate (PIP3) an antagonize the PI3-K/Akt pathway. It is believed that PTEN downregulation is a key factor contributing to the development of chemotherapy resistance and recurrence of various human tumors [108]. PTEN is known to regulate many cellular processes including growth, adhesion, migration, invasion, and apoptosis [11,86]. Nuclear factor kappa B (NF-κB) is known to upregulate anti-apoptotic genes such as *bcl-x*L and X-linked inhibitor of apoptosis (*XIAP*) leading to induce cell survival. Activation of NF-κB was observed in many types of cancer and was shown to contribute to apoptosis resistance in cancer cells [109]. In case of NF-κB expression, control HeLa cells without treatment showed a high expression of NF-κB. After treatment with CDF and the formulations, NF-κB levels in HeLa were decreased. Higher downregulation of NF-κB in HeLa cells was found when cells treated with the targeted formulation SPIONs@FA-PAMAM-CDF (decreased by 1.3 folds as compared to control) as compared to the non-targeted

formulation SPIONs@PAMAM-CDF (decreased by 1.19 folds as compared to control), indicating a better anticancer activity of the targeted formulation. In case of PTEN expression, western blot results showed a significantly low expression of PTEN in control cells. However, there was an increase in PTEN expression in cells treated with CDF and both of the formulations. Noticeably, PTEN level in cells treated with the targeted formulation SPIONs@FA-PAMAM-CDF was higher than CDF and the non-targeted formulation SPIONs@PAMAM-CDF. As compared to control, PTEN expression was upregulated by 3.2 folds in HeLa treated with the targeted formulation; whereas, in HeLa treated with free CDF and the non-targeted formulation, PTEN expression was increased by 1.58 and 2.14 folds, respectively [Fig 8]. The results suggested the ability of the targeted formulation SPIONs@FA-PAMAM-CDF to upregulate PTEN and downregulate NF-κB, which is known to play an important role in tumor suppressor activity and cancer cell death.

Summary

In this study, theranostic nanoparticles for cancer imaging and therapy were successfully fabricated with SPIONs in the core and FA-PAMAM conjugates on the periphery. To our knowledge, this is the first study employing a simple and efficient carbodiimide coupling chemistry to fabricate SPIONs decorated PAMAM dendrimers for MR imaging and targeted anticancer drug delivery. This fabrication method could be used to encapsulate different types of hydrophobic anticancer drugs for targeting MRI and therapy in various types of cancers by using appropriate targeting molecules for specific recognition of unique biomarkers overexpressed on cancer cells. In this study, the fabricated magnetic nanoparticles

SPIONs@FA-PAMAM showed great potential to be a promising MR contrast agent as well as an anticancer drug delivery system for CDF, a potent anticancer but highly lipophilic compound. The targeted nanoparticles SPIONs@FA-PAMAM possesses numerous favorable characteristics such as improved aqueous solubility of CDF, biological safety and targeting ability to cancer cells due to the presence of FA. As compared to SPIONs@PAMAM, SPIONs@FA-PAMAM showed a better ability to enhance MR contrast with a faster cellular uptake in *in vitro* T_2-weighted images and fluorescence microscopic studies. In addition, targeted formulation SPIONs@FA-PAMAM-CDF showed a higher anticancer activity, a higher percentage of apoptotic and necrotic cells with the ability to upregulate PTEN and downregulate NF-κB which could help overcome anticancer drug resistance and the recurrence of cancer after initial treatment. The results showed a promising potential of SPIONs@FA-PAMAM-CDF in targeted MRI and therapy in cancer, warranting further *in vivo* investigations underway in our laboratory.

REFERENCES

[1] C. Facts, American Cancer Society: Cancer Facts and Figures 2015, (2015). doi:10.3322/caac.21254.

[2] S. Mura, J. Nicolas, P. Couvreur, Stimuli-responsive nanocarriers for drug delivery., Nat. Mater. 12 (2013) 991–1003. doi:10.1038/nmat3776.

[3] D. Peer, J.M. Karp, S. Hong, O.C. Farokhzad, R. Margalit, R. Langer, Nanocarriers as an emerging platform for cancer therapy., Nat. Nanotechnol. 2 (2007) 751–760. doi:10.1038/nnano.2007.387.

[4] H. Maeda, J. Wu, T. Sawa, Y. Matsumura, K. Hori, Tumor vascular permeability and the EPR effect in macromolecular therapeutics: A review, J. Control. Release. 65 (2000) 271–284. doi:10.1016/S0168-3659(99)00248-5.

[5] P. Kesharwani, L. Xie, S. Banerjee, G. Mao, S. Padhye, F.H. Sarkar, A.K. Iyer, Hyaluronic acid-conjugated polyamidoamine dendrimers for targeted delivery of 3,4-difluorobenzylidene curcumin to CD44 overexpressing pancreatic cancer cells, Colloids Surfaces B Biointerfaces. 136 (2015) 413–423. doi:10.1016/j.colsurfb.2015.09.043.

[6] M.R. Liebowitz, M.B. Keller, Depression with anxiety and atypical depression, J. Clin. Psychiatry. 54 (1993) 10–15. doi:10.1002/ddr.

[7] P. Kesharwani, S. Banerjee, S. Padhye, F.H. Sarkar, A.K. Iyer, Parenterally administrable nano-micelles of 3,4-difluorobenzylidene curcumin for treating pancreatic cancer, Colloids Surfaces B Biointerfaces. 132 (2015) 138–145. doi:10.1016/j.colsurfb.2015.05.007.

[8] S. Padhye, S. Banerjee, D. Chavan, S. Pandye, K.V. Swamy, S. Ali, J. Li, Q.P. Dou, F.H. Sarkar, Fluorocurcumins as cyclooxygenase-2 inhibitor: Molecular docking, pharmacokinetics and tissue distribution in mice, Pharm. Res. 26 (2009) 2438–2445. doi:10.1007/s11095-009-9955-6.

[9] S. Padhye, H. Yang, A. Jamadar, Q.C. Cui, D. Chavan, K. Dominiak, J. McKinney, S. Banerjee, Q.P. Dou, F.H. Sarkar, New difluoro knoevenagel condensates of curcumin, their schiff bases and copper complexes as proteasome inhibitors and apoptosis inducers in cancer cells, Pharm. Res. 26 (2009) 1874–1880. doi:10.1007/s11095-009-9900-8.

[10] L. Li, F.S. Braiteh, R. Kurzrock, Liposome-encapsulated curcumin: In vitro and in vivo effects on proliferation, apoptosis, signaling, and angiogenesis, Cancer. 104 (2005) 1322–1331. doi:10.1002/cncr.21300.

[11] B. Bao, S. Ali, D. Kong, S.H. Sarkar, Z. Wang, S. Banerjee, A. Aboukameel, S. Padhye, P.A. Philip, F.H. Sarkar, Anti-tumor activity of a novel compound-CDF is mediated by regulating miR-21, miR-200, and pten in pancreatic cancer, PLoS One. 6 (2011) 1–12. doi:10.1371/journal.pone.0017850.

[12] B. Bao, S. Ali, S. Banerjee, Z. Wang, F. Logna, A.S. Azmi, D. Kong, A. Ahmad, Y. Li, S. Padhye, F.H. Sarkar, Curcumin analogue CDF inhibits pancreatic tumor growth by switching on suppressor microRNAs and attenuating EZH2 expression, Cancer Res. 72 (2012) 335–345. doi:10.1158/0008-5472.CAN-11-2182.

[13] P. Kesharwani, S. Banerjee, S. Padhye, F.H. Sarkar, A.K. Iyer, Hyaluronic Acid Engineered Nanomicelles Loaded with 3,4-Difluorobenzylidene

Curcumin for Targeted Killing of CD44+ Stem-Like Pancreatic Cancer Cells, Biomacromolecules. 16 (2015) 3042–3053. doi:10.1021/acs.biomac.5b00941.

[14] J.F. Kukowska-Latallo, K.A. Candido, Z. Cao, S.S. Nigavekar, I.J. Majoros, T.P. Thomas, L.P. Balogh, M.K. Khan, J.R. Baker, Nanoparticle Targeting of Anticancer Drug Improves Therapeutic Response in Animal Model of Human Epithelial Cancer, Cancer Res. 65 (2005) 5317–5324. doi:10.1158/0008-5472.can-04-3921.

[15] N. Malik, E.G. Evagorou, R. Duncan, Dendrimer-platinate: a novel approach to cancer chemotherapy, Anticancer Drugs. 10 (1999) 767–776. http://scholar.google.com/scholar?hl=en&btnG=Search&q=intitle:dendrimer-platinate:+a+novel+approach+to+cancer+chemotherapy#0.

[16] D. Luong, P. Kesharwani, R. Deshmukh, M.C.I. Mohd Amin, U. Gupta, K. Greish, A.K. Iyer, PEGylated PAMAM dendrimers: Enhancing efficacy and mitigating toxicity for effective anticancer drug and gene delivery., Acta Biomater. (2016) 1–16. doi:10.1016/j.actbio.2016.07.015.

[17] S. Ganta, H. Devalapally, A. Shahiwala, M. Amiji, A review of stimuli-responsive nanocarriers for drug and gene delivery, J. Control. Release. 126 (2008) 187–204. doi:10.1016/j.jconrel.2007.12.017.

[18] M. El-Sayed, M. Ginski, C. Rhodes, H. Ghandehari, Transepithelial transport of poly(amidoamine) dendrimers across Caco-2 cell monolayers, J. Control. Release. 81 (2002) 355–365. doi:S0168365902000871 [pii].

[19] Y. Matsumura, H. Maeda, A New Concept for Macromolecular Therapeutics

in Cancer Chemotherapy: Mechanism of Tumoritropic Accumulation of Proteins and the Antitumor Agent Smancs, Cancer Res. 46 (1986) 6387–6392. doi:10.1021/bc100070g.

[20] N. Malik, R. Wiwattanapatapee, R. Klopsch, K. Lorenz, H. Frey, J.W. Weener, E.W. Meijer, W. Paulus, R. Duncan, Dendrimers: Relationship between structure and biocompatibility in vitro, and preliminary studies on the biodistribution of 125I-labelled polyamidoamine dendrimers in vivo, J. Control. Release. 65 (2000) 133–148. doi:10.1016/S0168-3659(99)00246-1.

[21] N. Sato, H. Kobayashi, A. Hiraga, T. Saga, K. Togashi, J. Konishi, M.W. Brechbiel, Pharmacokinetics and enhancement patterns of macromolecular MR contrast agents with various sizes of polyamidoamine dendrimer cores, Magn. Reson. Med. 46 (2001) 1169–1173. doi:10.1002/mrm.1314.

[22] Y. Lu, P.S. Low, Folate-mediated delivery of macromolecular anticancer therapeutic agents, Adv. Drug Deliv. Rev. 64 (2012) 342–352. doi:10.1016/j.addr.2012.09.020.

[23] J. Holm, S.I. Hansen, M. HoierMadsen, P.E. Helkjaer, C.W. Nichols, Folate receptors in malignant and benign tissues of human female genital tract, Biosci. Rep. 17 (1997) 415–427. <Go to ISI>://A1997YE48100005.

[24] J.A.N. Holm, S.I. Hansen, M. Heier-madsen, P.E. Helkjser, C.W. Nichols, M.H.K. Sndergaard, M. Bzorek, C. Lines, J.F. Ross, P.K. Chaudhuri, M. Ratnam, D. Ph, J.A.N. Holm, S.I. Hansen, M. Her-madsen, P. Helkjer, M. Bzorek, Folate Receptors in Malignant and Benign Tissues of Human

Female Genital Tract, 17 (1993) 663–670.

[25] J. Holm, S.I. Hansen, M. Hoier-madsen, P.E. Helkjaer, M. Bzorek, Folate receptor in malignant effusions of ovarian carcinoma, Apmis. 103 (1995) 663–670. www.ncbi.nlm.nih.gov/pubmed/7488388.

[26] A.K. Iyer, G. Khaled, J. Fang, H. Maeda, Exploiting the enhanced permeability and retention effect for tumor targeting, Drug Discov. Today. 11 (2006) 812–818. doi:10.1016/j.drudis.2006.07.005.

[27] K. Greish, J. Fang, T. Inutsuka, A. Nagamitsu, H. Maeda, Macromolecular Therapeutics Tumour Targeting, Clin. Pharmacokinet. 42 (2003) 1089–1105.

[28] H. Maeda, T. Sawa, T. Konno, Mechanism of tumor-targeted delivery of macromolecular drugs, including the EPR effect in solid tumor and clinical overview of the prototype polymeric drug SMANCS, J. Control. Release. 74 (2001) 47–61. doi:10.1016/S0168-3659(01)00309-1.

[29] F. Yuan, M. Dellian, D. Fukumura, M. Leunig, D.A. Berk, R.K. Jain, V.P. Torchilin, Vascular Permeability in a Human Tumor Xenograft: Molecular Size Dependence and Cutoff Size, Cancer Res. 55 (1995) 3752–3756. doi:10.1038/nature02924.

[30] H. Maeda, The enhanced permeability and retention (EPR) effect in tumor vasculature: The key role of tumor-selective macromolecular drug targeting, Adv. Enzyme Regul. 41 (2001) 189–207. doi:10.1016/S0065-2571(00)00013-3.

[31] W. She, N. Li, K. Luo, C. Guo, G. Wang, Y. Geng, Z. Gu, Dendronized

heparin-doxorubicin conjugate based nanoparticle as pH-responsive drug delivery system for cancer therapy, Biomaterials. 34 (2013) 2252–2264. doi:10.1016/j.biomaterials.2012.12.017.

[32] L.M. Kaminskas, B.J. Boyd, C.J. Porter, Dendrimer pharmacokinetics: the effect of size, structure and surface characteristics on ADME properties, Nanomedicine. 6 (2011) 1063–1084. doi:10.2217/nnm.11.67.

[33] G. Orive, R.M. Hernández, A.R. Gascón, J.L. Pedraz, Micro and nano drug delivery systems in cancer therapy Review Article, Therapy. 3 (2005) 131–138.

[34] S.K. Sriraman, B. Aryasomayajula, V.P. Torchilin, Barriers to drug delivery in solid tumors., Tissue Barriers. 2 (2014) e29528. doi:10.4161/tisb.29528.

[35] J. Holm, S.I. Hansen, M. Høier-Madsen, K. Søndergaard, M. Bzorek, Folate receptor of human mammary adenocarcinoma., APMIS. 102 (1994) 413–419.

[36] J. Sudimack, R.J. Lee, Targeted drug delivery via the folate receptor., Adv. Drug Deliv. Rev. 41 (2000) 147–162. doi:10.1016/S0169-409X(99)00062-9.

[37] S.D. Konda, M. Aref, S. Wang, M. Brechbiel, E.C. Wiener, Specific targetig of folate-dendrimer MRI contrast agents to the high affinity folate receptor expressed in ovarian tunor xenographts, Magma. 12 (2001) 104–113.

[38] D.E. Sosnovik, E.A. Schellenberger, M. Nahrendorf, M.S. Novikov, T. Matsui, G. Dai, F. Reynolds, L. Grazette, A. Rosenzweig, R. Weissleder, L. Josephson, Magnetic resonance imaging of cardiomyocyte apoptosis with a novel magneto-optical nanoparticle, Magn. Reson. Med. 54 (2005) 718–724.

doi:10.1002/mrm.20617.

[39] S. Mornet, S. Vasseur, F. Grasset, E. Duguet, Magnetic nanoparticle design for medical diagnosis and therapy, Forunal Mater. Chem. 14 (2004) 2161–2175. doi:10.1039/b402025a.

[40] Y. Zhang, N. Kohler, M. Zhang, Surface modification of superparamagnetic magnetite nanoparticles and their intracellular uptake, Biomaterials. 23 (2002) 1553–1561. doi:10.1016/S0142-9612(01)00267-8.

[41] I. Safarik, M. Safarikova, Magnetic Nanoparticles and Biosciences, Monatshefte Für Chemie. 759 (2002) 737–759. doi:10.1007/978-3-7091-6740-3_1.

[42] D.K. Kim, Maria Mikhaylova, Yu Zhang, and Mamoun Muhammed, Protective Coating of Superparamagnetic Iron Oxide Nanoparticles, Chem. Mater. 15 (2003) 1617–1627. doi:10.1021/cm021349j.

[43] D. Artemov, Molecular magnetic resonance imaging with targeted contrast agents, J. Cell. Biochem. 90 (2003) 518–524. doi:10.1002/jcb.10660.

[44] Q.A. Pankhurst, J. Connolly, S.K. Jones, J.J. Dobson, Applications of magnetic nanoparticles in biomedicine, J. Phys. D. Appl. Phys. 36 (2003) R167. doi:10.1088/0022-3727/36/13/201.

[45] E. Duguet, S. Vasseur, S. Mornet, G. Goglio, A. Demourgues, J. Portier, F. Grasset, P. Veverka, E. Pollert, Towards a versatile platform based on magnetic nanoparticles for in vivo applications, 29 (2006) 581–586.

[46] A. Ito, M. Shinkai, H. Honda, T. Kobayashi, Medical application of functionalized magnetic nanoparticles., J. Biosci. Bioeng. 100 (2005) 1–11.

doi:10.1263/jbb.100.1.

[47] P.F. Renshaw, C.S. Owen, A.E. Evans, J.S. Leigh, IMMUNOSPECIFIC NMR CONTRAST AGENTS, (1986).

[48] Y. Okuhata, Delivery of diagnostic agents for magnetic resonance imaging, Adv. Drug Deliv. Rev. 37 (1999) 121–137. doi:10.1016/S0169-409X(98)00103-3.

[49] K.C. Barick, S. Singh, D. Bahadur, M.A. Lawande, D.P. Patkar, P.A. Hassan, Carboxyl decorated Fe3O4 nanoparticles for MRI diagnosis and localized hyperthermia, J. Colloid Interface Sci. 418 (2014) 120–125. doi:10.1016/j.jcis.2013.11.076.

[50] P. Sharma, S. Rana, K.C. Barick, C. Kumar, H.G. Salunke, P.A. Hassan, Biocompatible phosphate anchored Fe3O4 nanocarriers for drug delivery and hyperthermia, New J. Chem. 38 (2014) 5500–5508. doi:10.1039/C4NJ01431F.

[51] E.Q. Song, J. Hu, C.Y. Wen, Z.Q. Tian, X. Yu, Z.L. Zhang, Y.B. Shi, D.W. Pang, Fluorescent-magnetic-biotargeting multifunctional nanobioprobes for detecting and isolating multiple types of tumor cells, ACS Nano. 5 (2011) 761–770. doi:10.1021/nn1011336.

[52] Y. Ren, J.G. Rivera, L. He, H. Kulkarni, D.-K. Lee, P.B. Messersmith, Facile, high efficiency immobilization of lipase enzyme on magnetic iron oxide nanoparticles via a biomimetic coating., BMC Biotechnol. 11 (2011) 63. doi:10.1186/1472-6750-11-63.

[53] O. Veiseh, J.W. Gunn, M. Zhang, Design and fabrication of magnetic

nanoparticles for targeted drug delivery and imaging, Adv. Drug Deliv. Rev. 62 (2010) 284–304. doi:10.1016/j.addr.2009.11.002.

[54] T.S. Anirudhan, D. Dilu, S. Sandeep, Synthesis and characterisation of chitosan crosslinked-??-cyclodextrin grafted silylated magnetic nanoparticles for controlled release of Indomethacin, J. Magn. Magn. Mater. 343 (2013) 149–156. doi:10.1016/j.jmmm.2013.04.007.

[55] S. Laurent, D. Forge, M. Port, A. Roch, C. Robic, L. Vander Elst, R.N. Muller, Magnetic iron oxide nanoparticles: Synthesis, stabilization, vectorization, physicochemical characterizations and biological applications, Chem. Rev. 108 (2008) 2064–2110. doi:10.1021/cr068445e.

[56] J.L. Arias, V. Gallardo, S. a Gómez-Lopera, R.C. Plaza, a V Delgado, Synthesis and characterization of poly(ethyl-2-cyanoacrylate) nanoparticles with a magnetic core., J. Control. Release. 77 (2001) 309–321. doi:10.1016/S0168-3659(01)00519-3.

[57] M. Shimomura, T. Abe, Y. Sato, K. Oshima, T. Yamauchi, S. Miyauchi, Sugar-binding property of magnetite particles modified with dihydroxyborylphenyl groups via graft polymerization of acrylic acid, Polymer (Guildf). 44 (2003) 3877–3882. doi:10.1016/S0032-3861(03)00327-6.

[58] D. Tanyolaç, A.R. Özdural, Preparation of low-cost magnetic nitrocellulose microbeads, React. Funct. Polym. 45 (2000) 235–242. doi:10.1016/S1381-5148(00)00037-7.

[59] S.H. Wang, X. Shi, M. Van Antwerp, Z. Cao, S.D. Swanson, X. Bi, J.R. Baker, Dendrimer-Functionalized Iron Oxide Nanoparticles for Specific

Targeting and Imaging of Cancer Cells, Adv. Funct. Mater. 17 (2007) 3043–3050. doi:10.1002/adfm.200601139.

[60] U.O. Häfeli, G.J. Pauer, In vitro and in vivo toxicity of magnetic microspheres, J. Magn. Magn. Mater. 194 (1999) 76–82. doi:10.1016/S0304-8853(98)00560-5.

[61] R. Müller, H. Steinmetz, R. Hiergeist, W. Gawalek, Magnetic particles for medical applications by glass crystallisation, J. Magn. Magn. Mater. 272-276 (2004) 1539–1541. doi:10.1016/j.jmmm.2003.12.250.

[62] A.K. Gupta, M. Gupta, Synthesis and surface engineering of iron oxide nanoparticles for biomedical applications, Biomaterials. 26 (2005) 3995–4021. doi:10.1016/j.biomaterials.2004.10.012.

[63] C. Corot, P. Robert, J.M. Id??e, M. Port, Recent advances in iron oxide nanocrystal technology for medical imaging, Adv. Drug Deliv. Rev. 58 (2006) 1471–1504. doi:10.1016/j.addr.2006.09.013.

[64] H.-J. Weinmann, W. Ebert, B. Misselwitz, H. Schmitt-Willich, Tissue-specific MR contrast agents., Eur. J. Radiol. 46 (2003) 33–44. doi:10.1016/S0720-048X(02)00332-7.

[65] M. Babincová, P. Sourivong, D. Leszczynska, P. Babinec, Blood-specific whole-body electromagnetic hyperthermia., Med. Hypotheses. 55 (2000) 459–460. doi:10.1054/mehy.2000.1089.

[66] S. Wada, L. Yue, K. Tazawa, I. Furuta, H. Nagae, S. Takemori, T. Minamimura, New local hyperthermia using dextran magnetite complex (DM) for oral cavity: experimental study in normal hamster tongue., Oral Dis.

7 (2001) 192–195. doi:10.1034/j.1601-0825.2001.0070309.x.

[67] M. Arruebo, R. Fernández-pacheco, M.R. Ibarra, J. Santamaría, Magnetic nanoparticles Controlled release of drugs from nanostructured functional materials, Rev. Lit. Arts Am. 2 (2007) 22–32. doi:10.1016/S1748-0132(07)70084-1.

[68] J.W.M. Bulte, D.L. Kraitchman, Iron oxide MR contrast agents for molecular and cellular imaging, NMR Biomed. 17 (2004) 484–499. doi:10.1002/nbm.924.

[69] Y.-M. Huh, Y. Jun, H.-T. Song, S. Kim, J. Choi, J.-H. Lee, S. Yoon, K. Kim, J.-S. Shin, J.-S. Suh, J. Cheon, In vivo magnetic resonance detection of cancer by using multifunctional magnetic nanocrystals., J. Am. Chem. Soc. 127 (2005) 12387–12391. doi:10.1021/ja052337c.

[70] R. Weissleder, a Moore, U. Mahmood, R. Bhorade, H. Benveniste, E. a Chiocca, J.P. Basilion, In vivo magnetic resonance imaging of transgene expression., Nat. Med. 6 (2000) 351–355. doi:10.1038/73219.

[71] X. Shi, S.H. Wang, S.D. Swanson, S. Ge, Z. Cao, M.E. Van Antwerp, K.J. Landmark, J.R. Baker, Dendrimer-functionalized shell-crosslinked iron oxide nanoparticles for in-vivo magnetic resonance imaging of tumors, Adv. Mater. 20 (2008) 1671–1678. doi:10.1002/adma.200702770.

[72] D. Luong, P. Kesharwani, B.A. Killinger, A. Moszczynska, F.H. Sarkar, S. Padhye, A.K. Rishi, A.K. Iyer, Solubility enhancement and targeted delivery of a potent anticancer flavonoid analogue to cancer cells using ligand decorated dendrimer nano-architectures, J. Colloid Interface Sci. 484 (2016)

33–43. doi:10.1016/j.jcis.2016.08.061.

[73] M. García-Díaz, S. Nonell, Á. Villanueva, J.C. Stockert, M. Cañete, A. Casadó, M. Mora, M.L. Sagristá, Do folate-receptor targeted liposomal photosensitizers enhance photodynamic therapy selectivity?, Biochim. Biophys. Acta - Biomembr. 1808 (2011) 1063–1071. doi:10.1016/j.bbamem.2010.12.014.

[74] E. Mornet, N. Carmoy, C. Lainé, L. Lemiègre, T. Le Gall, I. Laurent, R. Marianowski, C. Férec, P. Lehn, T. Benvegnu, T. Montier, Folate-equipped nanolipoplexes mediated efficient gene transfer into human epithelial cells., Int. J. Mol. Sci. 14 (2013) 1477–501. doi:10.3390/ijms14011477.

[75] C.P. Leamon, P.S. Low, Membrane folate-binding proteins are responsible for folate-protein conjugate endocytosis into cultured cells., Biochem. J. 291 (Pt 3 (1993) 855–60. http://www.pubmedcentral.nih.gov/articlerender.fcgi?artid=1132447&tool=pmcentrez&rendertype=abstract.

[76] Y. Zhao, S. Liu, Y. Li, W. Jiang, Y. Chang, S. Pan, X. Fang, Y.A. Wang, J. Wang, Synthesis and grafting of folate-PEG-PAMAM conjugates onto quantum dots for selective targeting of folate-receptor-positive tumor cells, J. Colloid Interface Sci. 350 (2010) 44–50. doi:10.1016/j.jcis.2010.05.035.

[77] S. a McCarthy, G.-L. Davies, Y.K. Gun'ko, Preparation of multifunctional nanoparticles and their assemblies, Nat. Protoc. 7 (2012) 1677–1693. doi:10.1038/nprot.2012.082.

[78] R. Khodadust, G. Unsoy, S. Yalcın, G. Gunduz, U. Gunduz, PAMAM

dendrimer-coated iron oxide nanoparticles: synthesis and characterization of different generations, J. Nanoparticle Res. 15 (2013) 1488. doi:10.1007/s11051-013-1488-6.

[79] F. Gao, B.F. Pan, W.M. Zheng, L.M. Ao, H.C. Gu, Study of streptavidin coated onto PAMAM dendrimer modified magnetite nanoparticles, J. Magn. Magn. Mater. 293 (2005) 48–54. doi:10.1016/j.jmmm.2005.01.042.

[80] M.H. Mashhadizadeh, Drug-Carrying Amino Silane Coated Magnetic Nanoparticles as Potential Vehicles for Delivery of Antibiotics, J. Nanomed. Nanotechnol. 03 (2012) 3–9. doi:10.4172/2157-7439.1000139.

[81] M. Shen, H. Cai, X. Wang, X. Cao, K. Li, S.H. Wang, R. Guo, L. Zheng, G. Zhang, X. Shi, Facile one-pot preparation, surface functionalization, and toxicity assay of APTS-coated iron oxide nanoparticles, Nanotechnology. 23 (2012) 105601. doi:10.1088/0957-4484/23/10/105601.

[82] Z.I. Patricia Anne A, Ignacio-de Leon, Size-selective molecular transport through silica colloidal nanopores., Chem. Commun. (Camb). 47 (2011) 553–555. doi:10.1039/c0cc02101f.

[83] P. Kesharwani, R.K. Tekade, N.K. Jain, Formulation development and in vitro-in vivo assessment of the fourth-generation PPI dendrimer as a cancer-targeting vector., Nanomedicine (Lond). (2014). doi:10.2217/nnm.13.210.

[84] A.K. Iyer, K. Greish, J. Fang, R. Murakami, H. Maeda, High-loading nanosized micelles of copoly(styrene-maleic acid)-zinc protoporphyrin for targeted delivery of a potent heme oxygenase inhibitor., Biomaterials. 28 (2007) 1871–81. doi:10.1016/j.biomaterials.2006.11.051.

[85] P. Kesharwani, R.K. Tekade, N.K. Jain, Generation dependent safety and efficacy of folic acid conjugated dendrimer based anticancer drug formulations., Pharm. Res. 32 (2015) 1438–1450. doi:10.1007/s11095-014-1549-2.

[86] S. Roy, Y. Yu, S.B. Padhye, F.H. Sarkar, A.P.N. Majumdar, Difluorinated-Curcumin (CDF) Restores PTEN Expression in Colon Cancer Cells by Down-Regulating miR-21, PLoS One. 8 (2013) 5–10. doi:10.1371/journal.pone.0068543.

[87] H.S. Yoo, T.G. Park, Folate-receptor-targeted delivery of doxorubicin nano-aggregates stabilized by doxorubicin-PEG-folate conjugate., J. Control. Release. 100 (2004) 247–56. doi:10.1016/j.jconrel.2004.08.017.

[88] N. Parker, M.J. Turk, E. Westrick, J.D. Lewis, P.S. Low, C.P. Leamon, Folate receptor expression in carcinomas and normal tissues determined by a quantitative radioligand binding assay., Anal. Biochem. 338 (2005) 284–93. doi:10.1016/j.ab.2004.12.026.

[89] P. Kesharwani, R.K. Tekade, V. Gajbhiye, K. Jain, N.K. Jain, Cancer targeting potential of some ligand-anchored poly(propylene imine) dendrimers: A comparison, Nanomedicine Nanotechnology, Biol. Med. 7 (2011) 295–304.

[90] P. Kesharwani, V. Mishra, N.K. Jain, Generation dependent hemolytic profile of folate engineered poly(propyleneimine) dendrimer, J. Drug Deliv. Sci. Technol. 28 (2015) 1–6. doi:10.1016/j.jddst.2015.04.006.

[91] W. Sun, S. Mignani, M. Shen, X. Shi, Dendrimer-based magnetic iron oxide

nanoparticles: Their synthesis and biomedical applications, Drug Discov. Today. 00 (2016) 1–13. doi:10.1016/j.drudis.2016.06.028.

[92] Z. Qiao, X. Shi, Dendrimer-based molecular imaging contrast agents, Prog. Polym. Sci. 44 (2015) 1–27. doi:10.1016/j.progpolymsci.2014.08.002.

[93] A.K. Sharma, A. Gothwal, P. Kesharwani, H. Alsaab, A.K. Iyer, U. Gupta, Dendrimer nanoarchitectures for cancer diagnosis and anticancer drug delivery, Drug Discov. Today. (2016). doi:10.1016/j.drudis.2016.09.013.

[94] Y. Wei, B. Han, X. Hu, Y. Lin, X. Wang, X. Deng, Synthesis of Fe3O4 nanoparticles and their magnetic properties, Procedia Eng. 27 (2012) 632–637. doi:10.1016/j.proeng.2011.12.498.

[95] J. Yang, Y. Luo, Y. Xu, J. Li, Z. Zhang, H. Wang, M. Shen, X. Shi, G. Zhang, Conjugation of Iron Oxide Nanoparticles with RGD-Modified Dendrimers for Targeted Tumor MR Imaging, ACS Appl. Mater. Interfaces. 7 (2015) 5420–5428. doi:10.1021/am508983n.

[96] P. Kesharwani, R.K. Tekade, N.K. Jain, Generation dependent safety and efficacy of folic Acid conjugated dendrimer based anticancer drug formulations., Pharm. Res. 32 (2015) 1438–50. doi:10.1007/s11095-014-1549-2.

[97] A.M. Morawski, G.A. Lanza, S.A. Wickline, Targeted contrast agents for magnetic resonance imaging and ultrasound, Curr. Opin. Biotechnol. 16 (2005) 89–92. doi:10.1016/j.copbio.2004.11.001.

[98] C.C. Berry, Possible exploitation of magnetic nanoparticle – cell interaction for biomedical applications, (2005) 543–547. doi:10.1039/b409715g.

[99] D.E. Sosnovik, R. Weissleder, Emerging concepts in molecular MRI, Curr. Opin. Biotechnol. 18 (2007) 4–10. doi:10.1016/j.copbio.2006.11.001.

[100] W.-M. Liu, Y.-N. Xue, N. Peng, W.-T. He, R.-X. Zhuo, S.-W. Huang, Dendrimer modified magnetic iron oxide nanoparticle/DNA/PEI ternary magnetoplexes: a novel strategy for magnetofection, J. Mater. Chem. 21 (2011) 13306. doi:10.1039/c1jm11460c.

[101] S. Chandra, M.D. Patel, H. Lang, D. Bahadur, Dendrimer-functionalized magnetic nanoparticles: A new electrode material for electrochemical energy storage devices, J. Power Sources. 280 (2015) 217–226. doi:10.1016/j.jpowsour.2015.01.075.

[102] S. Thakur, R.K. Tekade, P. Kesharwani, N.K. Jain, The effect of polyethylene glycol spacer chain length on the tumor-targeting potential of folate-modified PPI dendrimers, J. Nanoparticle Res. 15 (2013). doi:10.1007/s11051-013-1625-2.

[103] A.R. Hilgenbrink, P.S. Low, Folate receptor-mediated drug targeting: From therapeutics to diagnostics, J. Pharm. Sci. 94 (2005) 2135–2146. doi:10.1002/jps.20457.

[104] M. Ocak, A.G. Gillman, J. Bresee, L. Zhang, A.M. Vlad, C. M??ller, R. Schibli, W.B. Edwards, C.J. Anderson, H.M. Gach, Folate receptor-targeted multimodality imaging of ovarian cancer in a novel syngeneic mouse model, Mol. Pharm. 12 (2015) 542–553. doi:10.1021/mp500628g.

[105] G.L. Zwicke, G.A. Mansoori, C.J. Jeffery, Targeting of Cancer Nanotherapeutics, Nano Rev. 1 (2012) 1–11.

[106] P. Kesharwani, R.K. Tekade, N.K. Jain, Generation dependent cancer targeting potential of poly(propyleneimine) dendrimer, Biomaterials. 35 (2014) 5539–5548. doi:10.1016/j.biomaterials.2014.03.064.

[107] B. Vivo, X. Huang, L. Li, T. Liu, N. Hao, H. Liu, D. Chen, F. Tang, The Shape Effect of Mesoporous Silica Nanoparticles on Biodistribution , (2011) 5390–5399.

[108] Y. Nagata, K.H. Lan, X. Zhou, M. Tan, F.J. Esteva, A.A. Sahin, K.S. Klos, P. Li, B.P. Monia, N.T. Nguyen, G.N. Hortobagyi, M.C. Hung, D. Yu, PTEN activation contributes to tumor inhibition by trastuzumab, and loss of PTEN predicts trastuzumab resistance in patients, Cancer Cell. 6 (2004) 117–127. doi:10.1016/j.ccr.2004.06.022.

[109] G.P. Collett, F.C. Campbell, Overexpression of p65/RelA potentiates curcumin-induced apoptosis in HCT116 human colon cancer cells, Carcinogenesis. 27 (2006) 1285–1291. doi:10.1093/carcin/bgi368.

ABSTRACT

DENDRIMER-COATED IRON OXIDE THERANOSTIC NANOPARTICLES FOR CANCER IMAGING AND THERAPY

by

Duy Luong

December 2016

Advisor: Dr. Arun Iyer

Major: Pharmaceutical Sciences

Degree: Master of Science

The bleak prognosis for patients diagnosed with metastatic cancer along with the low therapeutic efficacy and the recurrence of cancer in conventional chemotherapy are prompting clinical medicine to adopt a new strategy to detect cancer in early stage and to deliver the anticancer drugs specifically to tumor site to enhance therapeutic efficiency and minimize side effects. The aim of this study is to design a theranostic nanocarrier consisting of iron oxide nanoparticles (SPIONs) for magnetic resonance imaging (MRI) and Polyamidoamine dendrimers conjugated with folic acid (FA-PAMAM) for active targeted delivery of a highly potent but extremely lipophilic anticancer compound 3,4-difluorobenzylidene diferuloylmethane (CDF). The resulting targeted nanoparticles SPIONs@FA-PAMAM-CDF showed a significantly enhanced MR contrast as compared to the non-targeted nanoparticles. When tested on SKOV3 (ovarian cancer cells) and HeLa (cervical cancer cells), the targeted nanoformulations showed a higher accumulation in cancer cells with a better anticancer activity, a larger population of apoptotic cells and the ability to upregulate tumor suppressor phosphatase and

tensin homolog (PTEN) and inhibit nuclear factor kappa B (NF-κB) which further confirmed the ability of the folate decorated nanoparticles for targeted MRI and anticancer drug delivery.

AUTOBIOGRAPHICAL STATEMENT

PUBLICATIONS

- **D. Luong**, P. Kesharwani, A.K. Iyer, Multifunctional dendrimer-coated iron oxide theranostic nanoparticles for magnetic resonance imaging and active targeting cancer cells, (Manuscript under preparation).
- P. Kesharwani, **D. Luong**, H. Alsaab, F.H. Sarkar, S. Padhye, A.K. Rishi, A.K. Iyer, Folic acid decorated polymeric micelles loaded with 3,4-difluorobenzylidene diferuloylmethane for targeting cervical and ovarian cancers, (Under review).
- **D. Luong**, P. Kesharwani, B.A. Killinger, A. Moszczynska, F.H. Sarkar, S. Padhye, A.K. Rishi, A.K. Iyer, Solubility enhancement and targeted delivery of a potent anticancer flavonoid analogue to cancer cells using ligand decorated dendrimer nano-architectures, J. Colloid Interface Sci. 484 (2016) 33–43.
- **D. Luong**, P. Kesharwani, R. Deshmukh, M.C.I. Mohd Amin, U. Gupta, K. Greish, A.K. Iyer, PEGylated PAMAM dendrimers: Enhancing efficacy and mitigating toxicity for effective anticancer drug and gene delivery., Acta Biomater. (2016) 1–16.
- Nguyen Thanh Ha, Le Minh Tri, Nguyen Thien Hai, **Duy Luong**, Le Nguyen Nguyet Minh, Ameliorate the solubility of Paclitaxel by forming the complex with Hydroxypropyl-β-Cyclodextrin, Y Hoc TP. Ho Chi Minh. 18 (2014) 359-367.

PRESENTATIONS

- “Folic acid-decorated polymeric nanomicelles for targeted delivery of a potent flavonoid analogue to folate receptors overexpressing cancers”, 2016 American Association of Pharmaceutical Scientists (AAPS) Annual Meeting and Exposition, Colorado Convention Center, Denver, November 13th – 17th 2016
- “Dendrimer-coated iron oxide nanoparticles for cancer imaging and therapy”, Graduate Student Research Day, Wayne State University, Detroit, Michigan, October 7th 2016
- “Multifunctional dendrimer-coated iron oxide theranostic nanoparticles for magnetic resonance imaging and cancer therapy”, Annual Research Forum, Wayne State University, Detroit, Michigan, October 5th 2016
- “Folic acid decorated polymeric micelles loaded with 3,4-difluorobenzylidene diferuloylmethane for targeting cervical and ovarian cancers”, Annual Research Forum, Wayne State University, Detroit, Michigan, October 5th 2016
- “Polyamidoamine dendrimer-coated superparamagnetic iron oxide theranostic nanoparticles for targeted cancer therapy and imaging”, Cancer Metabolism Symposium, University of Michigan, Ann Arbor, Michigan, May 25th 2016
- “Dendrimer-coated iron oxide theranostic nanoparticles for cancer imaging and therapy”, Annual Research Forum, Wayne State University, Detroit, Michigan, November 4th 2015